

LJMU Research Online

Sharma, Y, Sollerman, J, Meynardie, W, Fremling, C, Das, KK, Yun, G, Kulkarni, SR, Schulze, S, Wise, J, Brennan, SJ, Brink, TG, Coughlin, MW, Dekany, R, Graham, MJ, Hinds, KR, Karambelkar, V, Kasliwal, MM, Li, ML, Nolan, K, Perley, DA, Purdum, JN, Rose, S, Rusholme, B, Sit, T, Tzanidakis, A, Wold, A, Yan, L and Yao, Y

Twin Peaks: SN 2021uvy and SN 2022hgk in the Landscape of Double-peaked Stripped Envelope Supernovae

<https://researchonline.ljmu.ac.uk/id/eprint/27296/>

Article

Citation (please note it is advisable to refer to the publisher's version if you intend to cite from this work)

Sharma, Y ORCID logoORCID: <https://orcid.org/0000-0003-4531-1745>,
Sollerman, J ORCID logoORCID: <https://orcid.org/0000-0003-1546-6615>,
Meynardie, W ORCID logoORCID: <https://orcid.org/0009-0001-6903-0131>,
Fremling, C ORCID logoORCID: <https://orcid.org/0000-0002-4223-103X>. **Das.**



























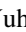

LJMU has developed **LJMU Research Online** for users to access the research output of the University more effectively. Copyright © and Moral Rights for the papers on this site are retained by the individual authors and/or other copyright owners. Users may download and/or print one copy of any article(s) in LJMU Research Online to facilitate their private study or for non-commercial research. You may not engage in further distribution of the material or use it for any profit-making activities or any commercial gain.

The version presented here may differ from the published version or from the version of the record. Please see the repository URL above for details on accessing the published version and note that access may require a subscription.

For more information please contact researchonline@ljmu.ac.uk

<http://researchonline.ljmu.ac.uk/>

Twin Peaks: SN 2021uvy and SN 2022hgk in the Landscape of Double-peaked Stripped Envelope Supernovae

Yashvi Sharma¹ , Jesper Sollerman² , William Meynardie³ , Christoffer Fremling⁴ , Kaustav K. Das¹ , Gene Yun⁵ ,
S. R. Kulkarni¹ , Steve Schulze⁶ , Jacob Wise⁷ , Seán J. Brennan² , Thomas G. Brink⁸ , Michael W. Coughlin⁹ ,
Richard Dekany⁴ , Matthew J. Graham¹ , K. R. Hinds⁷ , Viraj Karambelkar¹ , Mansi M. Kasliwal¹ , Maggie L. Li¹ ,
Kira Nolan¹ , Daniel A. Perley⁷ , Josiah N. Purdum⁴ , Sam Rose¹ , Ben Rusholme¹⁰ , Tawny Sit¹¹ ,
Anastasios Tzanidakis¹² , Avery Wold¹⁰ , Lin Yan⁴ , and Yuhan Yao^{8,13} 

¹ Division of Physics, Mathematics and Astronomy, California Institute of Technology, Pasadena, CA 91125, USA; yssharma@astro.caltech.edu

² Department of Astronomy, The Oskar Klein Center, Stockholm University, AlbaNova, 10691 Stockholm, Sweden

³ Department of Astronomy, University of Michigan, 1085 S. University Ave., Ann Arbor, MI 48109, USA

⁴ Caltech Optical Observatories, California Institute of Technology, Pasadena, CA 91125, USA

⁵ Loomis Laboratory of Physics, University of Illinois at Urbana-Champaign, 1110 W Green St Loomis Laboratory, Urbana, IL 61801, USA

⁶ Center for Interdisciplinary Exploration and Research in Astrophysics (CIERA), Northwestern University, 1800 Sherman Ave., Evanston, IL 60201, USA

⁷ Astrophysics Research Institute, Liverpool John Moores University, 146 Brownlow Hill, Liverpool L3 5RF, UK

⁸ Department of Astronomy, University of California, Berkeley, CA 94720-3411, USA

⁹ School of Physics and Astronomy, University of Minnesota, Minneapolis, MN 55455, USA

¹⁰ IPAC, California Institute of Technology, 1200 E. California Blvd, Pasadena, CA 91125, USA

¹¹ Department of Astronomy and Center of Cosmology and AstroParticle Physics, The Ohio State University, Columbus, OH 43210, USA

¹² Department of Astronomy and the DiRAC Institute, University of Washington, 3910 15th Avenue NE, Seattle, WA 98195, USA

¹³ Miller Institute for Basic Research in Science, 468 Donner Lab, Berkeley, CA 94720, USA

Received 2025 July 2; revised 2025 September 1; accepted 2025 September 3; published 2025 September 22

Abstract

In recent years, a class of stripped-envelope supernovae (SESNe) has emerged that show two distinct peaks in their light curves, where the first peak cannot be attributed to shock cooling emission. Such peculiar supernovae are often studied individually, explained by invoking some combination of powering mechanisms. However, they have seldom been discussed in the broader context of double-peaked SESNe. In this paper, we attempt to form a picture of the landscape of double-peaked SESNe and their powering mechanisms by adding two more objects—SN 2021uvy and SN 2022hgk. SN 2021uvy is a broad and luminous SN Ib with an unusually long rise of the first peak and constant color evolution with rising photospheric temperature during the second peak. Although its first peak is similar to that of SN 2019stc, their second peaks differ in properties, making it unique among double-peaked objects. SN 2022hgk shows striking photometric similarity to SN 2019cad and spectroscopic similarity to SN 2005bf, both of which have been suggested to be powered by a double-nickel distribution in their ejecta. We analyze their light curves and colors, compare them with a sample of other double-peaked published supernovae for which we have additional data, and analyze the light curve parameters of the sample. We observe a correlation (p -value ~ 0.025) between the peak absolute magnitudes of the first and second peaks. The sample shows variety in the photometric and spectroscopic properties, and thus no single definitive powering mechanism applies to the whole sample. However, sub-groups of similarity exist that can be explained by mechanisms like the double-nickel distribution, magnetar central engine, interaction, and fallback accretion. We also map out the duration between the peaks (Δt^{21}) versus the difference between peak absolute magnitudes (ΔM^{21}) as a phase-space that could potentially delineate the most promising powering mechanisms for the double-peaked SESNe.

Unified Astronomy Thesaurus concepts: Type Ib supernovae (1729); Type Ic supernovae (1730); Core-collapse supernovae (304)

1. Introduction

The number of observed stripped-envelope supernovae (SESNe) showing two distinct light-curve peaks has been

increasing in recent years with the advent of wide-field dynamic all-sky surveys. This emerging class of SESNe does not seem to form a homogeneous group, instead, there might be subgroups of objects that share observational similarities and powering mechanisms. A common subgroup is SESNe that show a fast initial decline ($t_{1/2} \lesssim 5$ days) and then develop a second (i.e. the main) peak that appears like a normal SESN. Such a rapidly declining first peak is often associated with the

shock-cooling phase from the extended envelope of the progenitor (Nakar & Piro 2014; Piro 2015; Piro et al. 2021) or very nearby circumstellar material (CSM, e.g., Jin et al. 2021; Khatami & Kasen 2024), and is commonly observed in Type IIb SNe (Morales-Garoffolo et al. 2015; Pellegrino et al. 2023; Crawford et al. 2025) but also some Type Ibc SNe (Taddia et al. 2016; Das et al. 2024). SESNe with early shock-cooling peaks also appear to show a strong correlation between the first and second peak absolute magnitudes, likely because both peak luminosities are related to the explosion energy (see Figure 1 of Das et al. 2024).

However, the rest of the double-peaked SESNe show large heterogeneity in light curve shapes, luminosities, and spectral properties, sometimes varying between the two peaks of the same supernova. Such objects have often been studied individually and compared to a few similar, previously known SNe, and various combinations of powering mechanisms have been invoked. The commonly used powering mechanisms include (see Section 4.2 for specific examples, references and discussion): (i) double-nickel distribution, (ii) delayed magnetar energy injection, (iii) interaction with circumstellar material (CSM), (iv) energy injection due to fallback accretion, (v) eruptive precursor powering the initial peak, and (vi) pulsational pair-instability eruptions. For a few SNe, tell-tale signs of the powering mechanism are present in the observations, such as narrow emission lines in the optical spectra (indicating CSM interaction). However, for many double-peaked SESNe, a number of these scenarios, or combinations thereof, can reasonably fit the light curve data well. More seldom have these supernovae been analyzed as a photometric class, but doing so might reveal pockets of homogeneity in this dispersed group of objects that perhaps correlate to a particular powering mechanism. Several of the invoked powering mechanisms also have their own limitations on the brightness of the peaks they can produce, the duration between the two peaks, or other observables that can help differentiate between the mechanisms (see Section 4.2).

Gathering more observations of such peculiar supernovae can be particularly important given the rarity of the objects themselves and the exceptional nature of some of the proposed models. Collecting a larger sample also improves our ability to group these objects systematically based on light-curve similarity. In this paper, we present an extensive analysis of SN 2021uvy—a bright, slowly evolving double-peaked SN Ib, and SN 2022hgk—a moderate luminosity and duration double-peaked SN Ib, which we have followed as part of the Zwicky Transient Facility (ZTF) survey and were previously mentioned in the sample study by Das et al. (2024). We compare these two supernovae with a sample of clearly double-peaked, published SNe Ibc, mainly from the ZTF archive (see Section 3.1). For this double-peaked SESNe sample, we estimate several light-curve parameters and attempt to infer whether any phase space mapped out by these parameters can

be useful for discerning the possible powering mechanisms of these objects.

This paper is organized as follows. In Section 2, we present the observations of the two SNe and data processing methods. In Section 3, we compare the light curves, colors, bolometric luminosities, and spectra of the two SNe with other similar double-peaked SESNe from the literature. We define a sample of clearly double-peaked SESNe from the ZTF archive in Section 3.1, analyze their light curve parameters in Section 4.1, and discuss the landscape of powering mechanisms for this sample in Section 4.2. Finally, we summarize our results in Section 5.

2. Observations

2.1. Discovery

2.1.1. SN 2021uvy

SN 2021uvy (a.k.a. ZTF21abmldj) is located at J2000.0 coordinates $\alpha = 00^{\text{h}}29^{\text{m}}30^{\text{s}}.88$ and $\delta = +12^{\circ}06'21''.01$ in a faint host galaxy (SDSS r band 22.2 mag). The redshift is determined to be $z = 0.0944$ from one of our intermediate resolution spectra at late times (Section 2.4). SN 2021uvy was first detected in the ZTF survey (Bellm et al. 2019; Graham et al. 2019; Dekany et al. 2020) data on 2021 August 4 (MJD 59403.424) at a host-subtracted magnitude of 20.64 in the ZTF r band and was reported (Fremling 2021) to the Transient Name Server (TNS¹⁴) by the Bright Transient Survey (BTS; Fremling et al. 2020; Perley et al. 2020; Rehemtulla et al. 2024) team. The SN was caught at an early stage and has good photometric coverage before and during the rise. It was initially reported as a superluminous supernova (SLSN) candidate (Lunnan et al. 2021) and initially classified as a SLSN-I at $z \sim 0.255$ (Poidevin et al. 2021) based on the top SNID (Blondin & Tonry 2007) match of a spectrum obtained on 2021 August 13 with SPRAT (Pascik et al. 2014) on the Liverpool Telescope (LT; Steele et al. 2004). It was reclassified as SN Ibc at $z = 0.1$ (Ridley et al. 2021) by the ePESSTO team (Smartt et al. 2015; Chen 2019) using a higher resolution spectrum obtained also on 2021 August 13 with EFOSC2 (Buzzoni et al. 1984) on ESO’s New Technology Telescope, which removed its superluminous candidacy. Finally, it was classified as a SN Ib-pec (peculiar) by the BTS team (Chu et al. 2021) based on a spectrum obtained with the LRIS (Oke et al. 1995; Perley 2019) spectrograph on the Keck-I telescope on 2021 September 9. SN 2021uvy was interesting as a luminous Type Ib supernova with an unusually long ~ 50 days rise to the peak ($M_{pk}^1 \approx -19.8$). It became even more peculiar when it brightened again after declining for ~ 25 days post-peak. The rise of the second peak was also slow (~ 30 days) and attained a similar luminosity as the first peak

¹⁴ <https://www.wis-tns.org>

($M_{pk}^2 \approx -19.3$). We obtained follow-up optical imaging and spectroscopic observations until the SN faded below apparent magnitude $m_r = 22.7$.

2.1.2. SN 2022hgk

SN 2022hgk (a.k.a. ZTF22aaezyos) is located at J2000.0 coordinates $\alpha = 14^h10^m23^s70$ and $\delta = +44^\circ14'01''.21$ in the host galaxy SDSS J141023.70+441401.8. The redshift is determined to be $z=0.0335$ from a host-galaxy spectrum obtained after the SN faded. SN 2022hgk was first detected in ZTF data on 2022 April 6 (MJD 59675.344) at a host-subtracted r -band magnitude of 20.76 and reported to TNS (Fremling 2022). The transient remained fainter than 19 mag for the next ~ 25 days and, thus, was not assigned for follow-up under the BTS survey criteria. Spectroscopic follow-up was triggered only once the transient started brightening again and developed a second peak, and SN 2022hgk was subsequently classified as a SNIb by the BTS team (Perley et al. 2022) based on a spectrum obtained with the SEDM spectrograph (Ben-Ami et al. 2012; Blagorodnova et al. 2018) on the Palomar 60 inch telescope on 2022 May 20. We continued follow-up optical imaging and spectroscopy until the SN faded below 21 mag.

2.2. Optical Photometry

For both of these SNe, we obtained forced point-spread function photometry from the ZTF forced photometry service (Masci et al. 2019, 2023) in g , r , and i bands and from the ATLAS forced photometry service (Tonry et al. 2018; Smith et al. 2020) in c and o bands. Additional optical photometry was obtained with the Rainbow camera on the Palomar 60 inch telescope (Cenko et al. 2006), the Optical wide-field camera (IO:O) on LT, ALFOSC on the Nordic Optical Telescope (NOT), and the imaging camera on the Katzman Automatic Imaging Telescope (KAIT) at Lick Observatory. The data from P60 and KAIT were processed with the automatic image subtraction pipeline FPIPE (Fremling et al. 2016). The data from LT were processed with custom image subtraction and analysis software (K. Hinds & K. Taggart et al. 2025, in preparation), and the photometry was measured using PSF fitting techniques from Fremling et al. (2016). The data from NOT were reduced with PyNOT¹⁵ data reduction pipeline, image subtraction to remove host contribution was performed with HOTPANTS version 5.11 (Becker 2015) using a pre-supernova r band image from the DESI Legacy Imaging Surveys (LS; Dey et al. 2019), and the aperture photometry was calibrated against a set of stars from the DESI Legacy Imaging Surveys.

All photometry presented in this paper is corrected for Milky Way extinction using the Python package extinction

(Barbary 2016), the dust extinction law from Fitzpatrick (1999), the Schlafly & Finkbeiner (2011) dust map, $E(B - V) = 0.067$ mag for SN 2021uvy, $E(B - V) = 0.005$ mag for SN 2022hgk, and $R_V = 3.1$ for both SNe. All measurements are converted into flux units for the analysis. The luminosity distances (and in turn, distance moduli and absolute magnitudes) are calculated using the cosmology parameters from Planck Collaboration et al. (2020) ($H_0 = 67.7$, $\Omega_m = 0.31$, $\Omega = 1$). The absolute magnitudes are calculated using a distance modulus (DM) of 38.254 for SN 2021uvy and 35.879 for SN 2022hgk and are K-corrected. Given the absence of NaID narrow absorption in spectra of both SNe and the faint host galaxy of SN 2021uvy, we do not account for any host reddening. The optical photometry data are included in Appendix A and shown in Figure 1.

2.3. Swift Ultraviolet/Optical Telescope Photometry

The field of SN 2022hgk was observed with the Ultraviolet/Optical Telescope (Roming et al. 2005) (UVOT) aboard the Swift satellite (Gehrels et al. 2004) between MJD = 59720.72 and 59732.38 in bands $w2$, $m2$, $w1$, u , b , and v . We retrieved science-ready data from the Swift archive.¹⁶ The all-sky exposures for a given epoch and filter were co-added to boost the signal-to-noise ratio using `uvotimsum` in HEASOFT¹⁷ version 6.31.1. We measured the brightness of the SN with the Swift tool `uvotsource`, setting the source aperture radius of $5''$ and a significantly larger background region. All measurements were calibrated with the latest calibration files and converted to the AB system following Breeveld et al. (2011). The UV photometry (not host-subtracted) is included in Appendix A. Since the UV photometry is not corrected for host contribution, we do not use it to construct the bolometric light curves.

2.4. Optical Spectroscopy

We obtained spectroscopic follow-up for SN 2021uvy between 2021 August 16 and 2023 July 23 and for SN 2022hgk between 2022 May 8 and 2022 July 27 with the following instruments:

1. Spectral Energy Distribution Machine (SEDM, $R \sim 100$, Blagorodnova et al. 2018) on P60, data processed using `pysedm` (Rigault et al. 2019; Kim et al. 2022).
2. Low Resolution Imaging Spectrometer (LRIS, $R \sim 800$ –1400, Oke et al. 1995) on the Keck-I telescope, data processed using `LPIPE` (Perley 2019).
3. Double Beam Spectrograph (DBSP, $R \sim 1000$, Oke & Gunn 1982) on the Palomar 200 inch telescope (P200),

¹⁶ https://www.swift.ac.uk/swift_portal

¹⁷ <https://heasarc.gsfc.nasa.gov/docs/software/heasoft/>

¹⁵ <https://github.com/jkrogager/PyNOT>

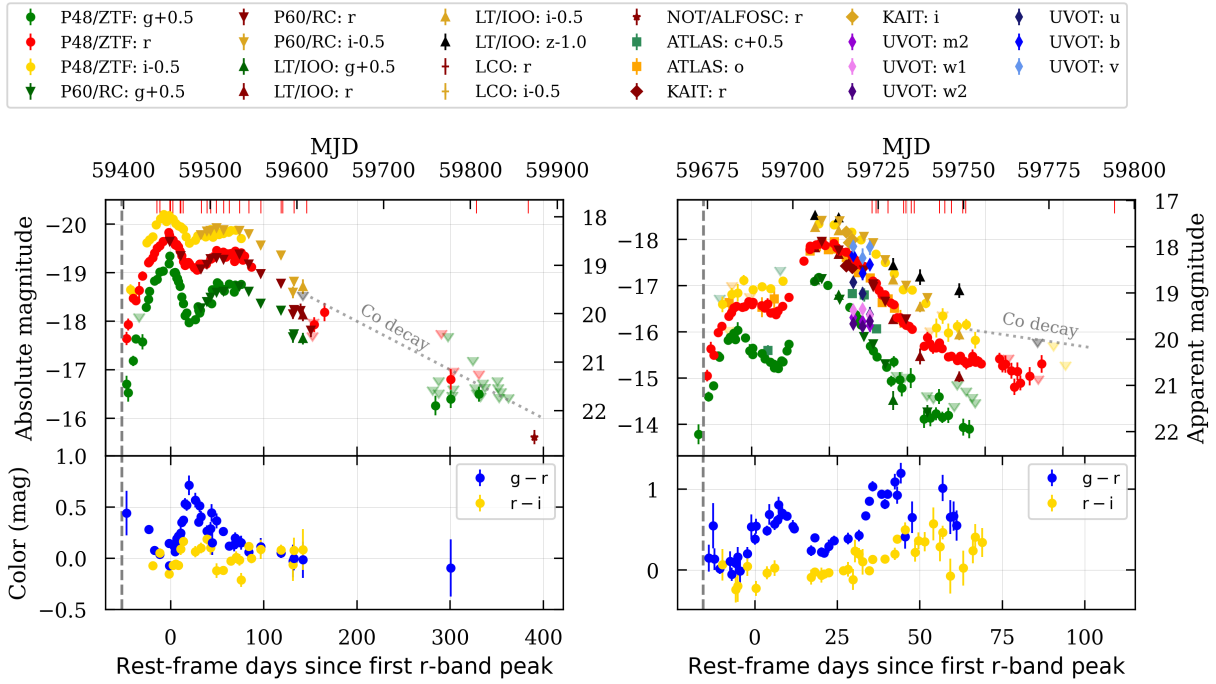


Figure 1. Light (top) and color (bottom) curves of SN 2021lvy (left) and SN 2022hgk (right). The 5σ detections are shown with solid markers and 3σ upper limits with transparent markers. All photometry is corrected for MW extinction. Absolute magnitudes are K-corrected (by adding $-2.5 \log_{10}(1+z)$) and obtained using Planck Collaboration et al. (2020) cosmology. The ^{56}Co decay rate (radioactive power) is shown with a dotted gray line. The spectral phases are marked on the top axis with red vertical lines. The explosion epochs are shown with gray dashed lines.

data processed using DBSP-DRP (Prochaska et al. 2020; Roberson et al. 2022).

4. Alhambra Faint Object Spectrograph and Camera (ALFOSC, $R \sim 360$), on the Nordic Optical Telescope (NOT), data processed using PyPeIt (Prochaska et al. 2020).
5. Spectrograph for the Rapid Acquisition of Transients (SPRAT, $R \sim 360$, Piascik et al. 2014) on the Liverpool Telescope (LT, Steele et al. 2004). Data processed using a custom Python pipeline utilizing the packages Astropy (Astropy Collaboration et al. 2022), NumPy (van der Walt et al. 2011), SciPy (Virtanen et al. 2020), and Matplotlib (Hunter 2007).

We present 23 spectra of SN 2021lvy in this paper (22 from the ZTF group, 1 from TNS, Ridley et al. 2021) covering epochs from -15 to 384 rest-frame days from its first peak in the r band and 14 spectra of SN 2022hgk covering epochs from 17 to 95 rest-frame days from its first peak in the r band. The spectral sequences are listed in Appendix B and shown in Figure 2. We also present spectra obtained as part of the ZTF follow-up campaigns of double-peaked SESNe in our sample (see Section 3.1 for details) that have not been published previously in Appendix B, namely SN 2020acct (11 spectra, -1 to 149 rest-frame days), SN 2021pkd (4 spectra, -7 to 7 days), and SN 2023plg (22 spectra, 70–147 days). All spectra

were corrected for Milky Way extinction using the same procedure as the photometry, then calibrated using contemporaneous host-subtracted ZTF data in the r band. All spectra will be made available on WISeREP (Yaron & Gal-Yam 2012).

3. Analysis

3.1. The Double-peaked SESN Sample

To collect the sample of previously published double-peaked SESNe in ZTF, we looked at ZTF light curves of all unambiguously classified SESNe (Type Ib, Ic, Ic-BL, Ib/c, Ib-pec) in the ZTF archive (a total of 501 objects). We obtained the light curves from Fritz (van der Walt et al. 2019; Coughlin et al. 2023) and interpolated them using Gaussian process regression. We then used `scipy.signal.find_peaks` functionality to search for prominent peaks in the r -band light curves (and g -band light curves in cases where r -band data were not available). We visually vetted the light curves that were identified to have >1 peak (46 out of 501) and rejected objects that: (i) had incorrect identification of multiple peaks due to missing coverage (and consequently incorrect interpolation), (ii) had more than two bumps/peaks (for example, SN 2021efd identified as a bumpy SN in Soraisam et al. 2022), or (iii) had non-prominent bumps and plateaus.

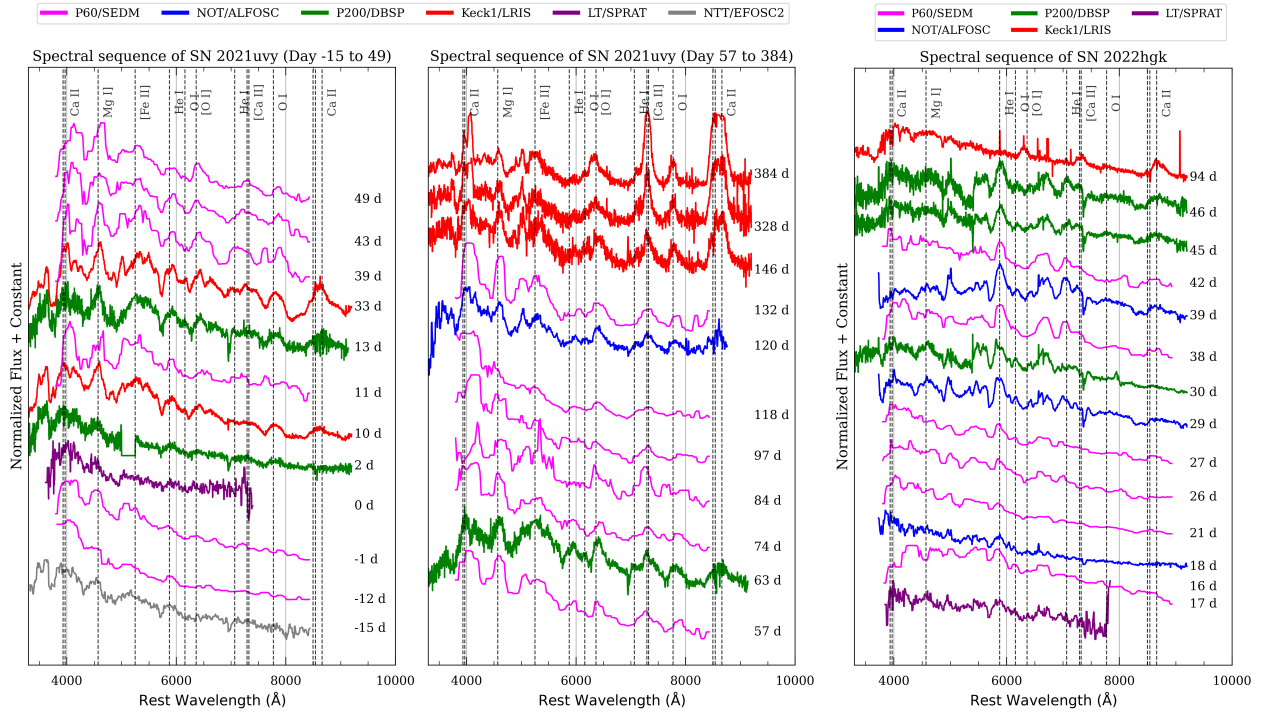


Figure 2. Spectral sequences of SN 2021uvy (left and center) covering epochs from -15 to 384 rest-frame days since its first peak and of SN 2022hgk (right) covering epochs from 17 to 95 rest-frame days since its first peak. Some characteristic spectral lines are marked with vertical gray dashed lines. Spectra are smoothed with a median filter of window size 5 .

Table 1
Sample of Published Double-peaked SESNe in the ZTF Archive

IAU Name	ZTF Name	Redshift	Type	$E(B - V)_{MW}$ (mag)	$E(B - V)_{host}$ (mag)	References
SN 2018ijp	ZTF18aceqrrs	0.0848	Ic	0.03	0.0	Tartaglia et al. (2021)
SN 2019cad	ZTF19aamsetj	0.02751	Ic	0.02	0.5 ^a	Gutiérrez et al. (2021)
SN 2019oys	ZTF19abucwzt	0.0162	Ib	0.09	0.0	Sollerman et al. (2020)
SN 2019stc	ZTF19acbonaa	0.1178	Ic/SLSN-I	0.08	0.18 ^b	Gomez et al. (2021)
SN 2020acct	ZTF20acwobku	0.0347	Ibc	0.03	0.0	Angus et al. (2024)
SN 2021pkd	ZTF21abfjlx	0.0398	Ib	0.04	0.0	Soraisam et al. (2022)
SN 2021uvy	ZTF21abmldj	0.0944	Ib	0.07	0.0	Das et al. (2024)
SN 2022hgk	ZTF22aaezyos	0.0335	Ib	0.01	0.0	Das et al. (2024)
SN 2022jli	ZTF22aapubuy	0.0055	Ic	0.04	0.25 ^c	Moore et al. (2023) ^d
SN 2022xxf	ZTF22abnvurz	0.0034	Ic-BL	0.04	0.8 ^e	Kuncarayakti et al. (2023)
SN 2023aew	ZTF23aaawbwc	0.025	Ibc	0.04	0.0	Kangas et al. (2024) ^f
SN 2023plg	ZTF23aaxuvkn	0.027	Ibc	0.06	0.0	Sharma et al. (2024)

Notes.

^a From Gutiérrez et al. (2021).

^b From Chen et al. (2023a).

^c From Chen et al. (2024).

^d Also Chen et al. (2024).

^e From Kuncarayakti et al. (2023).

^f Also Sharma et al. (2024).

We also rejected one object that fits the double-peak criteria but has not yet been published. SN 2022jli did not get filtered out with this methodology, as its first peak was not covered in

ZTF, but we added it to our sample since it is a known peculiar double-peaked supernova. The resulting sample (12 SNe) is summarized in Table 1, and includes SNe 2021uvy and

2022hgk. We note that SN 2019stc is classified as a luminous SN Ic in Gomez et al. (2021), but if host extinction is considered, it reaches superluminous status and is classified as a SLSN-I in Chen et al. (2023a). Thus, the observed fraction of clearly double-peaked Type Ibc SNe is $\sim 2.5\%$ of all Type Ibc SNe. In the following sections, we compare the photometric and spectroscopic properties of our two key objects, SNe 2021uvy and 2022hgk, with supernovae from this collected sample.

3.2. Light Curves

We fit the rise of SN 2021uvy in ZTF data with an exponential curve to constrain the explosion epoch, as the rise time is unusually long, but for SN 2022hgk, we fit the rise with a power-law curve. We converted the r , g , and i -band magnitudes into linear flux densities (in μJ), then used the Markov Chain Monte Carlo (MCMC) technique with the following equations to fit the exponential rise (1) and the power-law rise (2) in the bands separately:

$$f = f_{\text{max}} \left(1 - e^{-\frac{(t_{\text{exp}} - t)}{t_c}} \right) \quad (1)$$

$$f = a(t - t_{\text{exp}})^n \quad (2)$$

where f is the flux in μJ , and t is time (in MJD). We estimate t_{exp} (the explosion epoch), f_{max} (maximum flux), and t_c (characteristic rise-time) in Equation (1); and t_{exp} , a (proportionality constant), and n (power-law index) in Equation (2) using MCMC. We then calculate the mean and standard deviation of the best-fit values of t_{exp} obtained from the three ZTF bands to get the final explosion epoch at MJD 59398.21 ± 2.50 for SN 2021uvy and MJD 59673.80 ± 4.60 for SN 2022hgk.

Figure 1 shows the light- (top panel) and color- (bottom panel) curves of SN 2021uvy (left) and SN 2022hgk (right). Both objects show very conspicuous double-peaked light curves, which are highly unusual for SESNe. There are also obvious differences in luminosities and timescales. SN 2021uvy's first peak is broad and has a very slow rise of 52 rest-frame days from explosion to a peak absolute magnitude of $M_{pk,r}^1 = -19.8$ in the r band. It then declines for 25 rest-frame days at a rate of $0.030 \pm 0.002 \text{ mag day}^{-1}$ in the r band, faster than the radioactive Co-decay rate ($\approx 0.01 \text{ mag day}^{-1}$). After a clear minimum at around MJD 59480, SN 2021uvy brightens again for ~ 28 rest-frame days to an absolute magnitude of $M_{pk,r}^2 = -19.3$ (slightly fainter than the first peak), then slowly declines at a rate of $0.011 \pm 0.001 \text{ mag day}^{-1}$, very close to the decay rate of ^{56}Co , shown by the gray dotted line in Figure 1 (left).

On the other hand, SN 2022hgk is nearly two magnitudes fainter at maximum luminosity than SN 2021uvy, has an overall shorter duration and a more luminous second peak compared to the first peak, unlike SN 2021uvy. SN 2022hgk

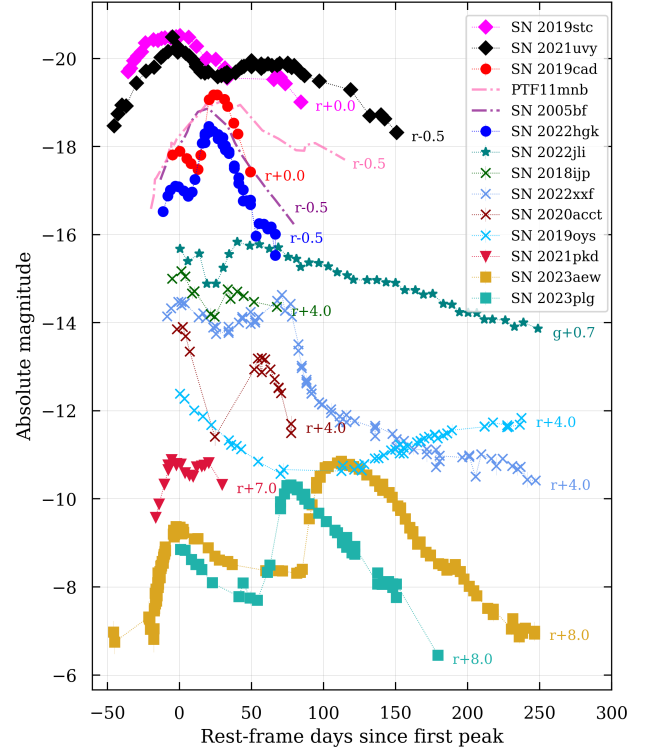


Figure 3. Light curves (r -band) of our sample of double-peaked SESNe, shifted vertically for clarity and with their first peaks aligned. Also shown for comparison are SN 2005bf and PTF11mnb (dash-dot lines). All absolute magnitudes have been calculated using the same cosmology.

has a first rise time of ~ 16 rest-frame days from explosion to a peak absolute magnitude of $M_{pk,r}^1 = -16.6$, after which it slightly declines for only ~ 7 rest-frame days before brightening again to a peak absolute magnitude of $M_{pk,r}^2 = -17.9$. The peak-to-peak duration (Δt^{21} , more details in Section 4.1) in the r band for SN 2022hgk is ~ 22 rest-frame days compared to ~ 66 days for SN 2021uvy. The final decline of SN 2022hgk proceeds at a rate of $0.078 \pm 0.002 \text{ mag day}^{-1}$ in the r band until around MJD 59750, after which the decline appears to become slower and similar to the Co decay rate.

In Figure 3, we show the absolute r -band light curves of our double-peaked sample, along with the r -band light curves of peculiar double-peaked SNe like SN 2005bf (Type Ib; Anupama et al. 2005; Folatelli et al. 2006; Maeda et al. 2007) and PTF11mnb (Type Ic; Taddia et al. 2018). We obtained the light curves of SNe in our sample following Section 2.2 and binned them into 3 days bins. The absolute magnitudes of all SNe shown were calculated using the same cosmology (see Section 2.2), and host-galaxy extinction was taken into account wherever available. The light curves have been shifted horizontally to align their first peaks and shifted vertically for clarity.

Immediately, we can deduce from Figure 3 that there is significant diversity across the sample, but also sub-groups that

Table 2
Light Curve Parameters of Our Double-peaked SESN Sample

SN	Band	$t_{\text{rise},1/2}^1$ (days)	M_{pk}^1 (mag)	MJD $_{pk}^1$	$t_{\text{fade},1/2}^1$ (days)	$t_{\text{rise},1/2}^2$ (days)	M_{pk}^2 (mag)	MJD $_{pk}^2$	$t_{\text{fade},1/2}^2$ (days)	Δt^{21} (days)	ΔM^{21} (mag)
2018ijp	<i>r</i>	8.1 ± 0.3	-19.16 ± 0.13	58438	>9.2	>18.4	-18.67 ± 0.08	58481	33.7 ± 1.0	39.6	0.49
2019cad	<i>r</i>	>7.8	-17.87 ± 0.09	58567	>7.8	7.7 ± 0.2	-19.17 ± 0.03	58593	13.2 ± 0.5	25.3	-1.30
2019oys	<i>r</i>	...	-16.35 ± 0.05	58723	22.7 ± 0.9	111.6 ± 1.4	-15.74 ± 0.02	58982	277.5 ± 12.7	254.9	>0.6
2019stc	<i>r</i>	34.0 ± 0.7	-20.52 ± 0.05	58799	29.3 ± 1.0	>20.6	-19.60 ± 0.06	58876	>17.0	68.9	0.92
2020acct	<i>r</i>	>2.9	-18.06 ± 0.03	59196	6.6 ± 0.4	3.9 ± 0.1	-17.21 ± 0.01	59253	13.7 ± 0.4	55.1	0.85
2021pkd	<i>r</i>	12.0 ± 0.6	-17.84 ± 0.06	59394	>6.7	>10.6	-17.80 ± 0.05	59414	>12.5	19.2	0.04
2021uvy	<i>g</i>	22.6 ± 1.0	-19.80 ± 0.09	59455	10.8 ± 0.9	43.9 ± 0.1	-19.24 ± 0.02	59531	56.1 ± 0.6	69.4	0.56
	<i>r</i>	25.6 ± 1.9	-19.77 ± 0.08	59455	20.0 ± 0.7	>41.1	-19.37 ± 0.01	59528	55.6 ± 0.4	66.7	0.40
2022hgk	<i>g</i>	5.5 ± 0.4	-16.44 ± 0.05	59684	11.9 ± 0.4	6.4 ± 0.4	-17.63 ± 0.02	59712	10.7 ± 0.3	27.1	-1.20
	<i>r</i>	11.8 ± 0.7	-16.61 ± 0.13	59691	>5.8	7.7 ± 0.1	-17.92 ± 0.01	59713	14.8 ± 0.5	21.3	-1.31
2022jli	<i>g</i>	...	-16.37 ± 0.01	59708	>17.9	12.6 ± 0.7	-16.54 ± 0.04	59750	73.0 ± 3.9	41.8	>-0.2
2022xxf	<i>r</i>	>8.0	-18.47 ± 0.01	59880	>24.9	33.9 ± 2.1	-18.66 ± 0.02	59950	9.0 ± 0.1	69.8	-0.19
2023aew	<i>r</i>	11.7 ± 0.1^a	-17.28 ± 0.01	59959	34.6 ± 0.5	19.5 ± 0.1	-18.84 ± 0.01	60075	32.2 ± 0.1	113.2	-1.50
2023plg	<i>r</i>	...	-16.83 ± 0.02	60170	>22.1	7.8 ± 0.1	-18.30 ± 0.02	60249	23.1 ± 0.6	76.9	>-1.5

Notes. The rise and fade times are calculated between peak flux and half-of-peak flux. The superscripts “1” and “2” denote the first and second peak parameters, respectively. The rise times, fade times, and duration between the two peaks (Δt^{21}) are reported in rest-frame days.

^a Derived from TESS-Red band data.

share some light curve properties. The slow rise, peak luminosity, and first decline of SN 2021uvy are similar to what is seen for SN 2019stc, a luminous SESN (Gomez et al. 2021; Chen et al. 2023a). Gomez et al. (2022) mentions that the first peaks of both SNe 2019stc and 2021uvy fit well to a combined magnetar central engine and ^{56}Ni radioactive decay power model, but have weaker magnetar engines than typical SLSNe. They posit that this could explain the SLSNe-like light curve but normal SESNe-like spectra of SN 2019stc. However, this combined model does not account for the rebrightening and cannot explain the second peaks of these two SNe. SN 2022hgk’s *r*-band light curve and color curve are remarkably similar to those of SN 2019cad, also considered analogous to SN 2005bf and PTF11mnb. The luminosities and timescales of the two peaks of this group of objects, especially the initial rise before the first peak, which is >10 days from the explosion, fit the double-nickel distribution scenario (Folatelli et al. 2006; Bersten et al. 2013; Orellana & Bersten 2022) well. The final declines of these objects have some variation, with PTF11mnb and SN 2022hgk possibly showing a bump toward the end. The group of SESNe with confirmed CSM interaction signatures (SN 2018ijp—hydrogen-rich dense shell, SN 2019oys—hydrogen-rich CSM and high-ionization coronal lines, SN 2020acct—narrow emission lines during first peak, and SN 2022xxf—late-time narrow emission lines) are shown with crosses in Figure 3 and display the most variety in their light curve evolution, with some having ultra-long durations than others. The accretion-powered SN 2022jli is entirely unique, showing periodic undulations in its long decline. SN 2023aew and 2023plg both have widely separated peaks with a plateau connecting the two peaks and appear unlike

any of the other SNe in the sample. Finally, SN 2021pkd does not share a strong similarity with any of the other SNe.

Table 2 shows the light-curve parameters (luminosities at both peaks, rise and decline times in different filters measured from peak flux to half of the peak flux) for the double-peaked SESN sample. These parameters were all consistently estimated from interpolated ZTF light curves of the listed SNe when available (TESS-Red band data from Sharma et al. 2024 were used for the first-peak of SN 2023aew, and ASAS-SN *g*-band data from Chen et al. 2024 were used for the first-peak of SN 2022jli). The interpolation was performed using Gaussian process regression with the help of the HAFNET Python package (Yang & Sollerman 2023). We are collecting all these parameters in order to map out the landscape of double-peaked SESNe in terms of observable properties, and the ranges and distributions of these properties might later be valuable to constrain the viable powering mechanisms for their light curves. The grouping seen in Figure 3 is also apparent from this table, with some groups (e.g., SNe 2019stc, 2021uvy) having long rest-frame duration between the two peaks (Δt^{21}) and a fainter second peak ($\Delta M^{21} = M_{pk}^2 - M_{pk}^1 > 0$), while others (e.g., SNe 2019cad, 2022hgk) having shorter Δt^{21} and brighter second peak ($\Delta M^{21} < 0$). SNe 2023aew and 2023plg sit independently in this phase space, with a longer duration like the first group and a brighter second peak like the second.

3.3. Bolometric Luminosities

We used Superbol (Nicholl 2018) to calculate the pseudo-bolometric luminosity and bolometric luminosity for SN 2021uvy using its ZTF *gri* data and for SN 2022hgk using its ZTF *gri* and ATLAS *co* data. The other bands are first

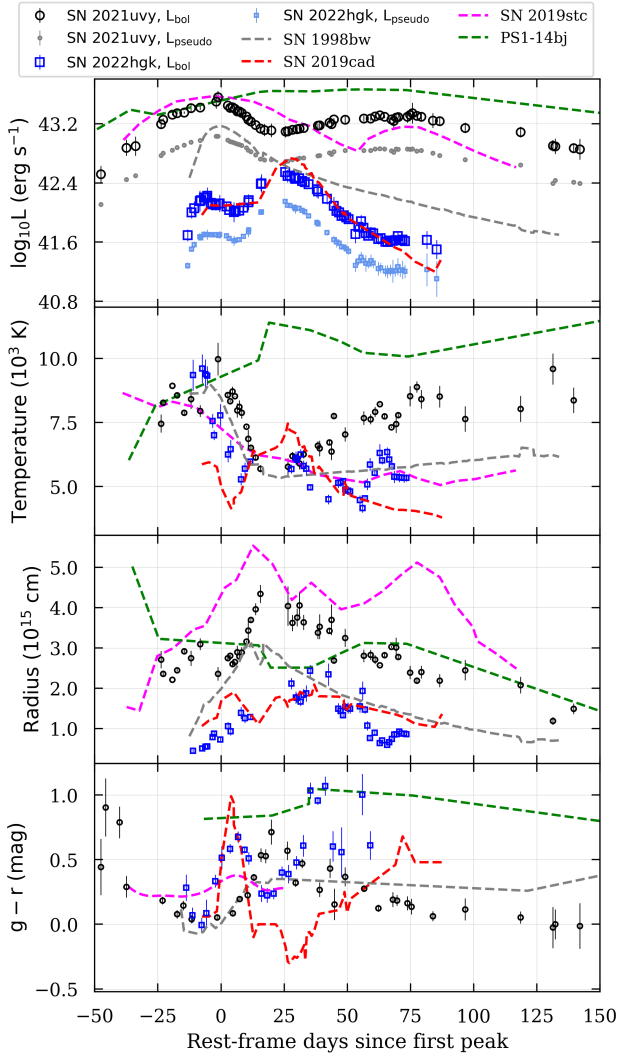


Figure 4. Evolution of the bolometric luminosity (top), blackbody temperature (second), blackbody radius (third), and $g - r$ color (bottom) with time of SN 2021uvy (black circles) and SN 2022hgk (blue squares). Shown for comparison are SN 2019cad (red), SN 2019stc (magenta), PS1-14bj (green), and SN 1998bw (gray). SN 2021uvy and SN 2019stc show similar evolution during their first light-curve peaks but diverge in behavior during the second peaks. SN 2021uvy develops a gradual rise in temperature during the second peak, similar to PS1-14bj, which also correlates with the lack of color evolution for both these SNe. The properties of SN 2022hgk closely resemble those of SN 2019cad.

interpolated to r -band epochs, and then the pseudo-bolometric luminosity is calculated by integrating the fluxes over the bandpasses at each epoch. The bolometric luminosity is estimated from the pseudo-bolometric luminosity by adding blackbody corrections (absorbed UV and near-infrared). Figure 4 shows the bolometric luminosity (top panel), estimated blackbody temperature (second panel), estimated blackbody radius (third panel), and $g - r$ color (bottom panel) for SNe 2019cad, 2019stc, 2021uvy, and 2022hgk, along with

the regular Type Ic-BL SN 1998bw, and a slow-evolving single-peaked SLSN-I PS1-14bj (chosen for comparison as it also shows no color evolution during its decline). The data for SN 1998bw were obtained with Superbol using its UBVR light curves (Galama et al. 1998; Patat et al. 2001; Sollerman et al. 2002). For SN 2019cad, only bolometric luminosity has been presented in Gutiérrez et al. (2021) and not temperature or radius; therefore, we use the *groiz* light curves from Gutiérrez et al. (2021) and Superbol to calculate the shown data (we did not correct for host-extinction due to its high uncertainty). The data for SN 2019stc were obtained from Gomez et al. (2021, their Figure 5) (they did not correct for host-extinction, although it is estimated in Chen et al. 2023a for SN 2019stc), and the data for PS1-14bj were obtained from Lunnan et al. (2016, their Figures 7 and 8).

Figure 4 shows that the first peaks of SN 2019stc and SN 2021uvy follow each other closely in bolometric luminosity, blackbody temperature, radius, and color. From the explosion until the end of the first decline (minima between the two peaks), both SNe show a consistent decrease in temperature (from $\sim 10,000$ K to ~ 5000 K), an increase in radius, getting bluer during the rise and becoming redder during the first decline (which is typical of stripped-envelope supernovae powered by ^{56}Ni , see SN 1998bw in gray). The similarity between SN 2019stc and SN 2021uvy stops at this point. For SN 2019stc, the temperature plateaus (like for SN 1998bw), and the radius follows the second brightening bump. However, for SN 2021uvy, the temperature starts rising rapidly along with no color evolution (like for PS1-14bj), staying around $g - r \approx 0$ mag until very late times (indicating some new energy injection). At the same time, its radius declines at a similar rate as for PS1-14bj and SN 1998bw. This might indicate that the powering mechanisms of the second peaks of SN 2019stc and SN 2021uvy are different. For SN 2019stc, both radioactive decay and delayed magnetar engine are disfavored according to Gomez et al. (2021), and an aspherical CSM, which could result in a lack of narrow lines, was instead favored for the second peak by those authors. We roughly estimate the ^{56}Ni mass (M_{Ni}) and ejecta mass (M_{ej}) assuming that the first peaks of SNe 2019stc and 2021uvy are powered by radioactivity using the analytical expressions from Khatami & Kasen (2019). This gives $M_{\text{Ni}}^{2019\text{stc}} \approx 1.9 M_{\odot}$, $M_{\text{Ni}}^{2021\text{uvy}} \approx 2.3 M_{\odot}$, $M_{\text{ej}}^{2019\text{stc}} \approx 10 M_{\odot}$, and $M_{\text{ej}}^{2021\text{uvy}} \approx 17 M_{\odot}$. These values, as expected, are much too large compared to typical SESNe (Rodríguez et al. 2023) and inconsistent with neutrino-driven core-collapse models (Woosley et al. 2021), making radioactivity as the only powering mechanism unfeasible.

On the other hand, SN 2022hgk’s bolometric light curve almost exactly matches that of SN 2019cad (if not corrected for host extinction), except toward the very end, when SN 2022hgk shows a little bump before fading completely.

Table 3
Peak Bolometric and Pseudo-bolometric Luminosities and Estimated Radiated Energies in the two Peaks of Our Double-peaked SESN Sample

SN	Lightcurve	L_{pk}^1 (10^{43} erg s $^{-1}$)	L_{pk}^2 (10^{43} erg s $^{-1}$)	E_{rad}^1 (10^{50} erg)	E_{rad}^2 (10^{50} erg)	E_{rad}^{total} (10^{50} erg)
2018ijp	Bolometric	~ 1.5	~ 0.6	~ 0.3	~ 0.7	~ 1.1
2019cad	Bolometric	0.13 ± 0.02	0.59 ± 0.07	0.008 ± 0.001	0.114 ± 0.005	0.139 ± 0.006
2019oys	Bolometric	>0.12	0.10 ± 0.39	>0.03	0.405 ± 0.296	0.436 ± 0.294
2019stc	Bolometric	~ 3.7	~ 1.4	~ 1.82	~ 0.52	~ 2.38
2020acct	Bolometric	0.96 ± 0.06	0.35 ± 0.01	~ 0.07	~ 0.04	~ 0.15
2021pkd	Bolometric	0.85 ± 1.13	0.34 ± 0.09	0.092 ± 0.018	0.059 ± 0.007	0.154 ± 0.019
2021uvy	Pseudo-bolometric	1.08 ± 0.03	0.72 ± 0.04	0.371 ± 0.004	0.764 ± 0.015	1.160 ± 0.016
	Bolometric	3.88 ± 0.77	2.30 ± 0.76	1.070 ± 0.037	2.244 ± 0.181	3.367 ± 0.183
2022hgk	Pseudo-bolometric	0.05 ± 0.01	0.14 ± 0.01	0.007 ± 0.001	0.037 ± 0.001	0.045 ± 0.001
	Bolometric	0.18 ± 0.05	0.35 ± 0.10	0.021 ± 0.001	0.095 ± 0.006	0.117 ± 0.006
2022jli	Pseudo-bolometric	~ 0.3	~ 0.4	~ 0.05	~ 0.29	~ 0.35
2022xxf	Bolometric	~ 0.9	~ 1.3	~ 0.22	~ 0.42	~ 0.67
2023aew	Bolometric	0.07 ± 0.00	1.20 ± 0.20	0.096 ± 0.005	0.560 ± 0.013	0.656 ± 0.018
2023plg	Bolometric	>0.19	0.67 ± 0.04	>0.04	0.218 ± 0.004	0.258 ± 0.008

Note. The superscripts “1” and “2” denote the first and second peaks, respectively. SN 2021uvy has $\sim 32\times$ more energy radiated than SN 2022hgk (shown in bold).

The temperature mirrors the luminosity and decreases sharply during the first decline (same as SNe 1998bw, 2019cad, 2019stc, 2021uvy), shows a small rise during the second brightening (like SN 2019cad, SN 2021uvy), decreases again during the second decline (like SN 2019cad), and rises at the very end (coincident with the final luminosity bump). SN 2022hgk’s radius only shows a rise and a decline, peaking around the second (and brightest) luminosity maximum. SN 2022hgk’s $g - r$ color becomes progressively redder during the second decline, as expected, and has a similar evolution to the $g - r$ color of SN 2019cad.

In Table 3, we have collected bolometric (and in some cases pseudo-bolometric when the bolometric estimate is not provided) luminosities at the two light-curve peaks and the estimated total radiated energies (E_{rad}) to crudely compare the energetics across the sample. We integrate bolometric light curves of SNe 2019cad, 2019oys, 2021pkd, 2021uvy, 2022hgk, and 2023plg obtained using Superbol and ZTF light curves to estimate the radiated energies and use the Monte-Carlo method to estimate the uncertainties on radiated energies as follows. We sample 1000 random points per epoch from a normal distribution that has the epoch luminosity as the mean and the uncertainty on the luminosity as the σ . We integrate the sampled light curves over the rest-frame days and take the mean and standard deviation of the resulting energy estimates. For SN 2023aew, we list the values reported in Sharma et al. (2024) that have been estimated using the same process described above. For SNe 2018ijp, 2019stc, 2020acct, 2022jli, and 2022xxf, we integrate the bolometric (or pseudo-bolometric) light curves obtained from Tartaglia et al. (2021, their Figure 2), Gomez et al. (2021, their Figure 5), Angus et al. (2024, their Figure 9), Chen et al. (2024, Figure 4), and

Kuncarayakti et al. (2023, their Figure A.1), respectively. We simply consider points from the first detection to the local minimum between the two peaks for calculating the energy radiated in the first peak and from the local minimum to the last detection for calculating the energy radiated in the second peak. This provides the simplest lower limits for the radiated energies, as we are not fitting any specific powering mechanisms to the light curves.

3.4. Spectral Comparison

Figure 5 compares the spectra obtained near the first (left panel) and second (right panel) peaks of SNe 2021uvy and 2022hgk with the most similar double-peaked SESNe from the sample. The first-peak spectra of SN 2021uvy have normal SESN features and look similar to those of SN 2019stc and PS1-14bj. SN 2021uvy shows He I $\lambda 5876$ signatures from the pre-peak epochs (Figure 2, left) which classifies it as a Type Ib. From the absorption minima of O I $\lambda 7774$ in the day 10 spectrum, we estimate an ejecta velocity of ~ 8000 km s $^{-1}$, which is also consistent with the He I absorption minimum. The lines of Ca II $\lambda\lambda 3934, 3969$, Mg I $\lambda 4571$, and O I $\lambda 7774$ appear to be of similar strength in these three SNe. The Fe II complex between 5000 Å and 5600 Å has more flux on the blue side and appears broader in SN 2021uvy than for SN 2019stc and PS1-14bj. SN 2021uvy and PS1-14bj also appear to have a slightly bluer continuum than SN 2019stc past the first peak. Overall, SN 2021uvy’s first peak exhibits Type Ib nature spectrally but with a slow-evolving SLSN-like light curve that hints toward a mixed powering mechanism (radioactivity + magnetar) as suggested by Gomez et al. (2021, 2022).

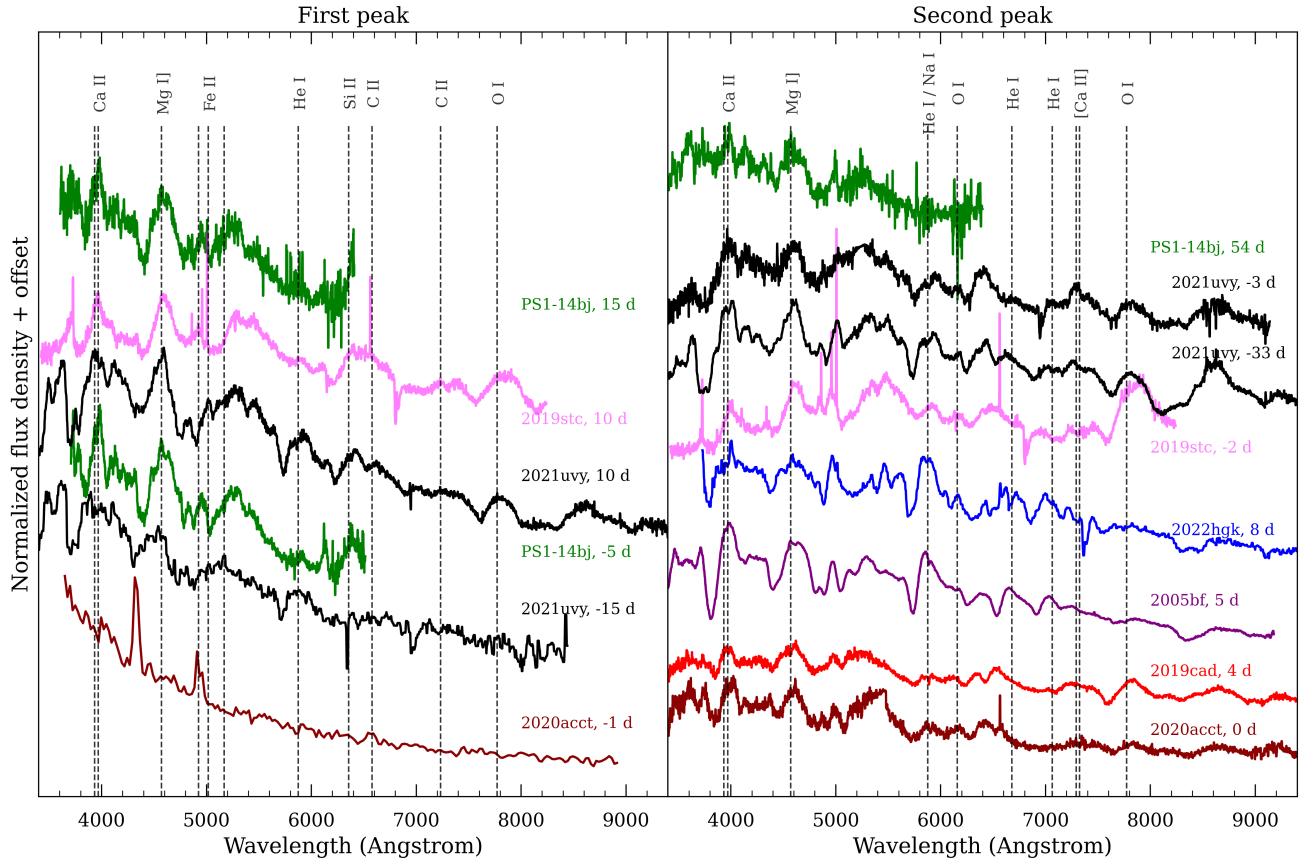


Figure 5. Left: First-peak spectra of SN 2021uvy (black) compared with those of SNe 2019stc (magenta), 2020acct (brown), and PS1-14bj (green), with phases reported with respect to the first peak. Similar to normal SESNe, the first-peak spectra of SNe 2019stc, 2021uvy and PS1-14bj are dominated by Ca II, Mg I, Fe II and O I. SN 2020acct, on the other hand, shows signs of CSM interaction at this phase. Right: Second-peak spectra of SNe 2021uvy (black) and 2022hgk (blue) compared with those of SNe 2005bf (purple), 2019cad (red), 2019stc (magenta), 2020acct (brown), and PS1-14bj (green), with phases reported with respect to the second peak (except for PS1-14bj). SN 2022hgk shows a close spectroscopic resemblance to the peculiar Type Ib SN 2005bf around their main (second) peaks. All spectra are smoothed with a median filter of window size 5 (except for SN 2020acct).

Other double-peaked SESNe that exhibit normal SESN spectra during the first peak include SNe 2019cad, 2022jli, and 2022xxf. However, SN 2022jli evolved into having accretion-powered second peak (Chen et al. 2024), and SN 2022xxf developed subtle H/He-free signs of CSM interaction (Kuncarayakti et al. 2023). SN 2023aew changed its type from SN II during the first peak to SN Ic during its second peak and then to having hydrogen reappear during the nebular phase, which could be due to hidden CSM interaction with a complex geometry (Sharma et al. 2024). SN 2020acct showed some early flash-ionization features, a sign of brief CSM interaction during the first peak (Angus et al. 2024), confirming its power source. This is to say that the sample of double-peaked SESNe show as much variety in their spectral nature as they do in their light curves and intermediate resolution spectra taken at crucial epochs in the light-curve evolution (early rise, peak, minima between peaks, second peak, and nebular) are necessary to enable the identification of

the powering mechanism. Unfortunately, for SN 2022hgk, no first-peak spectra were taken as it remained below the threshold for triggering follow-up as part of the BTS survey.

Looking at the right panel of Figure 5, around the second peak, the broad features of SNe 2019cad, 2019stc, 2020acct, and 2021uvy are similar and post-peak SESN-like but redder than PS1-14bj. The Ca NIR bumps also become prominent in SNe 2019cad, 2020acct, and 2021uvy. SN 2021uvy also has emission around 7300 Å which could possibly be [Ca II] + [O II], which is unusual for typical SESNe in photospheric phase, but has been observed in SNe 2019stc, 2020acct, 2023aew, and also 2018ibb (Schulze et al. 2024) as noted in Angus et al. (2024). Angus et al. (2024) also noted the striking similarity of the second-peak spectra of SNe 2020acct and 2023aew. SN 2022hgk shows strong He I lines at this epoch ($\sim 10,000 \text{ km s}^{-1}$) and a blue continuum. The SN 2022hgk spectrum at 7 days after the second peak closely resembles SN 2005bf's spectrum at 5 days past the second

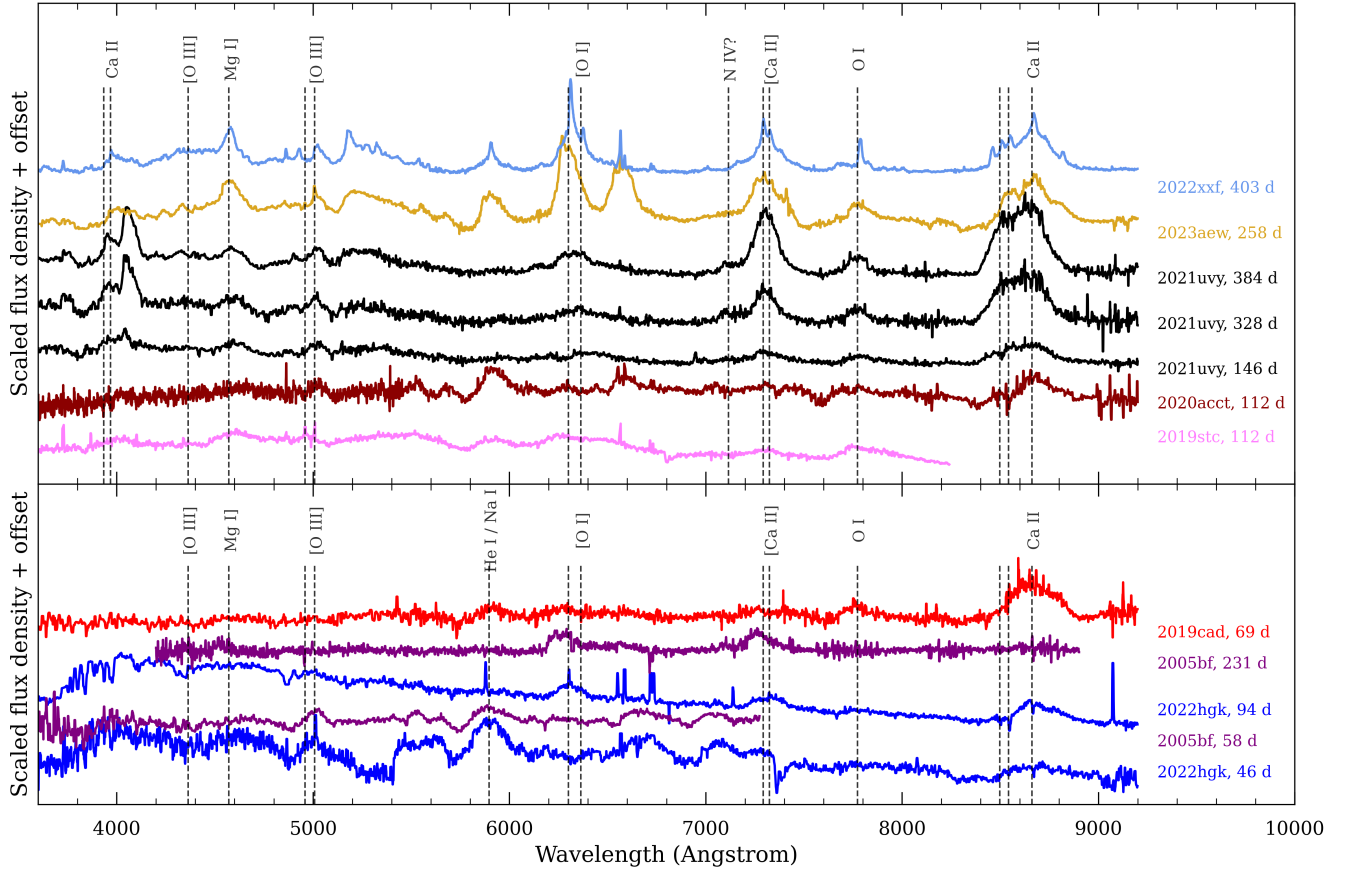


Figure 6. Top: Comparison of nebular spectra of SN 2021uvy (black) with SNe 2019stc (magenta), 2020acct (brown), 2022xxf (cornflowerblue) and 2023aew (gold). Bottom: Comparison of nebular spectra of SN 2022hgk (blue) with SNe 2005bf (purple) and 2019cad (red). All spectral phases are reported with respect to the first peak.

peak (Shivvers et al. 2019), with both showing He I lines and a lack of O I $\lambda 7774$. None of these SNe show obvious signs of interaction in their second peak spectra.

Figure 6 shows nebular (and near-nebular) spectra of some double-peaked SESNe, with the common nebular lines marked and some tentative line identifications. The phases shown are from the estimated time of the explosion. The final spectra available of SNe 2019stc and 2020acct are shown in the top panel and though they are not fully nebular, we can see [O I] $\lambda\lambda 6300, 6364$ and [Ca II] $\lambda\lambda 7292, 7324$ starting to appear. The spectra of SNe 2022xxf, 2023aew, and 2021uvy in the top panel have slight differences that could allude to their origin. Narrow lines become discernible in the nebular spectra of SN 2022xxf, revealing the H/He-free CSM interaction. SN 2023aew shows strong emission at the location of $H\alpha$, which appears to be too strong to be the [N II] nebular emission seen in many Type IIb/Ib (Barmantloo et al. 2024; Sharma et al. 2024) and instead could be re-emerged $H\alpha$, revealing the hidden CSM powering the supernova. However, the [Ca II]/[O I] flux ratio in these SNe (2021uvy ~ 1.18 ,

2022xxf ~ 1.16 , 2023aew ~ 0.8 , 2022hgk ~ 0.92 , 2005bf ~ 0.90) are similar, indicating similar oxygen core masses and in turn similar progenitors. SN 2021uvy shows strong emission lines around ~ 4000 Å which could be Ca II H&K lines but appear to be redshifted. The [Ca II] line in SN 2021uvy maintains a Gaussian profile with time, but [O I] seems to become flat-topped (similar to the case of Type Ib iPTF13bvn; Kuncarayakti et al. 2015), especially in the 384 days spectrum. This could be due to some asphericity in the ejecta (clumps or torus-like oxygen distribution as suggested in Taubenberger et al. 2009), or it could be due to absorption in the interior (Milisavljevic et al. 2010).

The bottom panel of Figure 6 compares SNe 2019cad and 2022hgk with SN 2005bf. The 46, 58, and 69 days spectra of SNe 2022hgk, 2005bf, and 2019cad, respectively, show hints of nebular emission lines but are not fully nebular. SN 2019cad differs from the other two SNe and shows stronger O I emission. SN 2022hgk at 46 days matches SN 2005bf at 58 days, maintaining the spectral similarities since their peaks. The 231 days spectrum of SN 2005bf shows its characteristic

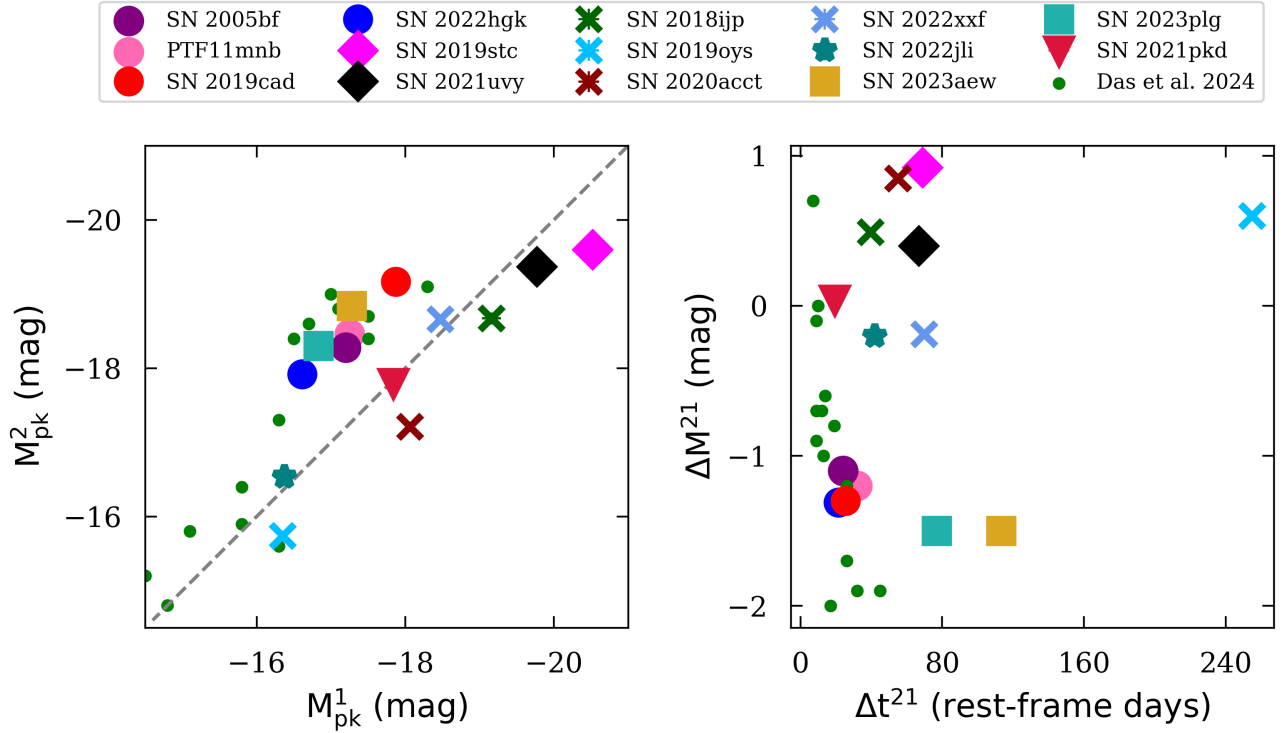


Figure 7. Left: Peak absolute magnitudes of the second peak vs. the first peak for the double-peaked SESN sample, and the shock-cooling powered double-peaked SESNe presented in Das et al. (2024). There appears to be a correlation between the peak magnitudes, which is strongest for the Das et al. (2024) SESNe (p -value $< 10^{-5}$) but also significant for our double-peaked SESN sample (p -value = 0.005). Right: Magnitude difference vs. rest-frame duration between the two peaks. Again, the potentially double-nickel powered SESNe form a tight group in this phase space.

blueshifted nebular lines, but the 94 days spectrum of SN 2022hgk does not, which is where SN 2022hgk finally differs from SN 2005bf. The blue continuum in SN 2022hgk at this phase is likely contamination from the host galaxy.

4. Discussion

4.1. Trends in the Double-peaked Light Curve Properties

The left panel of Figure 7 shows the r -band (g -band for SN 2022jli) absolute magnitudes of the second peak against those of the first peak (M_{pk}^2 versus M_{pk}^1), the right panel depicts the difference between the peak magnitudes against rest-frame duration between the peaks (ΔM^{21} versus Δt^{21}) for the double-peaked SESN sample discussed in this paper and for the sample of double-peaked Type Ibc SNe presented in Das et al. (2024). There appears to be a correlation between the absolute magnitudes of the first and second peaks (p -value = 0.005). The absolute magnitude correlation was observed by Das et al. (2024) for double-peaked SESNe that have the first peak attributed to cooling after the shock passes the extended envelope (or nearby CSM) of the progenitor. The mechanism behind such a correlation remains unclear. One possibility that Das et al. (2024) put forth is that SESNe with shock-cooling first peaks have He-star progenitors that shed

their envelopes in binary interactions shortly before exploding. For such progenitors, the first peak depends on the progenitor radius and the second peak on the ^{56}Ni mass. In both panels of Figure 7, SNe 2005bf, PTF11mnb, 2019cad, and 2022hgk (all potentially powered by double-nickel distributions, marked with circles) seem to form a group and lie in the same phase-space as the SESNe with shock-cooling peaks. The correlation in shock-cooling powered and double-nickel powered cases could also stem from both peaks being positively correlated with the explosion energy. SESNe with at least one of the peaks potentially powered by CSM interaction (marked with crosses) and the accretion-powered SN 2022jli (marked with a star) follow the correlation in the left panel but do not seem to form a group. Finally, SNe 2019stc and 2021uvy form a close duo in all panels.

It is apparent from Figure 7 that the location these supernovae occupy in the different phase spaces created by the light curve properties ($M_{pk}^2 - M_{pk}^1$, $\Delta M^{21} - \Delta t^{21}$, etc.) can help unveil the possible powering mechanisms, especially for models that have quantifiable restrictions on these light curve properties.

It is also possible that clear double-peaked SESNe with one peak significantly fainter than the other (i.e., that do not lie on

this correlation) lie outside the limiting magnitude of ZTF, and are thus being missed. The Vera C. Rubin Observatory and its Legacy Survey of Space and Time (LSST; Ivezić et al. 2019) will be able to identify such SESNe and help further populate these phase spaces.

4.2. Powering Mechanisms

The double-peaked stripped-envelope supernovae discussed so far exemplify the uncertainty about the powering mechanism of the light curves of this class. Normal SNe Ibc can be relatively well explained as being powered by the decay of radioactive ^{56}Ni that diffuses out of the initially optically thick ejecta. This self-contained explanation follows the simple model by Arnett (1982). It should be mentioned, however, that even this picture has been questioned in the literature. The ejecta masses deduced from some light curve analysis studies indicate values lower than anticipated from massive single stars (e.g., Taddia et al. 2015; Prentice et al. 2019) and the ^{56}Ni masses are too high to be explained by contemporary neutrino-driven core collapse models (Sollerman et al. 2022), spurring discussion on the need for other powering mechanisms even for the normal objects (e.g., Karamahmetoglu et al. 2023; Rodríguez et al. 2024). Analysis of the relationship between nebular line flux ratios ($[\text{Ca II}]/[\text{O I}]$) and ejecta masses estimated from light curve modeling (with Arnett 1982) of SESNe also revealed no or weak connection between the two, meaning both low and high ejecta mass objects have similar progenitors, implying the presence of other powering mechanisms responsible for the light-curve behavior of the more luminous SESNe (Fang et al. 2019; Prentice et al. 2022). Studying the rarer family of double-peaked objects has provided a plethora of suggestions, including the most common scenarios for powering the emission of supernovae. Often, different mechanisms or a combination thereof are invoked to explain each peak in such supernovae, although some modeling studies exist that try to explain the double-peaked light curve with a single mechanism. In the following sections, we briefly discuss the suggested powering mechanisms and attempt to form a picture of their diversity.

4.2.1. Double-nickel Distribution

An early suggestion for double-peaked SESNe was the notion of double nickel distributions. A jet-like structure that brings some radioactive material closer to the surface was proposed for the double-peaked peculiar Type Ib SN 2005bf (Folatelli et al. 2006), which would produce an early light curve peak before the central Ni power diffuses out on a longer time scale. SN 2019cad (analog of SN 2005bf) was proposed to have such a structure (Taddia et al. 2018; Gutiérrez et al. 2021, see also PTF11mnb), and the scenario was further explored (e.g., Orellana & Bersten 2022). This mechanism fits well given SN 2022hgk’s striking photometric similarity with

SN 2019cad and spectral similarity with SN 2005bf. It is clear from these models, however, that they have limited ability to match light-curve peaks that are well separated (large Δt^{21} and in turn delayed second peak that would be inconsistent with radioactive power diffusion timescale, like SNe 2019stc, 2020acct, 2021uvy, 2023aew), or with high luminosities (that require unreasonable nickel mass like SN 2019stc and SN 2021uvy), or that have more than two peaks, and the model is thus not generic enough to explain the full double peaked sample of SESNe.

4.2.2. Magnetar

The magnetar model has become popular for long-lived transients where the Arnett model yields unphysical ^{56}Ni masses, and is often invoked for peculiar SESNe (like SN 2005bf; Maeda et al. 2007), luminous SNe (Gomez et al. 2022) and superluminous supernovae (SLSNe, e.g., Chen et al. 2023b). The model offers a lot of flexibility in terms of rise times, peak luminosities, and duration—but does not naturally allow for double-peaked light curves or undulations. Chugai & Utrobin (2022) opposed the CSM-interaction scenario for the second peak of the luminous SN 2019stc as put forth in Gomez et al. (2021), and instead suggested a magnetar engine by invoking a less-understood dipole-field enhancement to allow for the second peak. Other similar suggestions, like magnetar flare activity, have been proposed in the context of wiggly light curves of SLSNe (Dong et al. 2023; Zhu et al. 2024), and Moriya et al. (2022) suggested that variations in the thermal energy injection from magnetar spin-down cause the light-curve bumps. However, Chugai & Utrobin (2022) only explains a single bump and does not identify any specific smoking-gun observables that could support the model. Moriya et al. (2022), on the other hand, predicts an increase in photospheric temperature coincident with the bumps and notes that SN 2019stc does not show such an increase. The only supernova in our sample that shows an increase in photospheric temperature for the second peak is SN 2021uvy, and therefore, could be an example of the magnetar thermal energy injection scenario. However, our temperature measurements only use *gri* bands, but UV data are required for a more accurate temperature estimate, and thus, this observation of temperature rise is tentative. The temperature rise in SN 2021uvy also appears to last throughout the entire duration of the second peak, implying that the increase in thermal energy injection would also need to be maintained for >100 days.

4.2.3. CSM

While some double-peaked SESNe have shown strong signs of interaction after the first peak that completely transform their spectra—for example, hydrogen-rich CSM interaction in SNe 2018ijp (Tartaglia et al. 2021) and 2019oys

(Sollerman et al. 2020); others have shown much more subtle but revealing signs of CSM interaction. One example of such a case is SN 2022xxf (Kuncarayakti et al. 2023), where the evidence for CSM interaction became obvious only at later times when narrow emission lines became more apparent in the optical spectra. The CSM must, in this case, be poor in both hydrogen and helium, which makes the configuration highly unusual (a detached CSM model was suggested for SN 2022xxf by Takei & Tsuna 2024). The analytical modeling by Chiba & Moriya (2024) explicitly mentions the possibility of modeling both of the peaks in the light curves of SNe 2005bf and 2022xxf using a flat density profile for the CSM. However, the model comes with the caveat that the duration between the two peaks (Δt^{21}) can be at most $\lesssim 100$ days, otherwise, the ejecta mass requirements become unphysical. Another caveat is that if the two peaks are too temporally separated (large Δt^{21}), the breakout luminosity (first peak) cannot be comparable to the luminosity of the second peak and thus the model has difficulty in explaining cases where first peak is brighter than the second peak (e.g., SN 2019stc). Khatami & Kasen (2024) explore different theoretical scenarios enabling a large variety of light curves from the CSM interaction powering only, including double-peaked light curves which in their modeling occur when the shock breaks out just outside the CSM edge (so that there is no continued interaction phase, see Khatami & Kasen 2024, their Figure 3) and the CSM is “heavy” (CSM mass \gtrsim ejecta mass, making the shock cooling phase more prominent). However, spectral signatures of such heavy CSM might be difficult to hide, thus making this scenario less likely for SESNe without any narrow line signatures. In the case of SN 2023aew (Kangas et al. 2024; Sharma et al. 2024), the $H\alpha$ P-Cygni feature seen during the first peak vanished at the time of the second peak and appeared again at later times, and the nebular lines showed a “horned” structure. These features, combined with the double-peaked light curve with large Δt^{21} , could be evidence that an aspherical or clumpy CSM powers the second peak of the supernova along with radioactive nickel decay, with the first peak being an eruptive precursor. SN 2023plg (Sharma et al. 2024) follows the light-curve behavior of SN 2023aew, and its second peak spectra share strong similarities with SN 2023aew’s second peak spectra (Sharma et al. 2024, their Figure 10), and could share the same powering mechanism.

4.2.4. Accretion

Another potential powering mechanism is accretion onto a compact object, where an accretion disk might form and efficiently convert energy to radiation. SN 2022jli (Moore et al. 2023; Chen et al. 2024)—the double-peaked SESN showing periodic undulations in its light curve during the second decline, was potentially powered by such a scenario.

Chen et al. (2024) advocated that the first peak might have been powered by a normal radioactive decay, whereas the second peak would be powered by mass accretion from the companion onto the newly formed compact object remnant. The second peak of this supernova was instead suggested to be powered by a magnetar (Section 4.2.2) by Cartier et al. (2024). In general, the different powering scenarios mentioned in these sections have been combined in a variety of different ways to explain double-peaked SESNe.

4.2.5. Pulsational Pair Instability Mechanism

Finally, we mention the suggestion put forward by Angus et al. (2024) for SN 2020acct, that the double-peaked light curve could have been powered by CSM interaction with a configuration from a pulsational pair instability supernova (PPISN; Barkat et al. 1967; Rakavy et al. 1967). PPI events cause extreme mass loss, and thus their ejecta CSM interactions can be quite luminous. The timing of the different events can vary depending on the specific evolution of the system and therefore provide models that can fit multiple well-separated peaks, explain precursors, and also bumpy light curves (Woosley 2017; Leung et al. 2019). However, clear identification of PPISNe is difficult as other powering mechanisms (and their combinations) could also fit the observations of peculiar multi-peaked SNe, and the surrounding CSM could also come from various mass-loss mechanisms (LBV eruptions, winds, etc.). The unique properties of SN 2020acct—hydrogen-poor interaction signatures during the first peak and a second peak showing terminal explosion SESN-like properties, together with an unfeasible nickel fraction ($f_{\text{Ni}} \sim 0.91$) from fitting radioactive decay power to the second peak, made it a possible PPISN candidate (Angus et al. 2024).

5. Summary

In this paper, we have presented optical photometry and spectroscopy of two double-peaked stripped envelope supernovae discovered by the Zwicky Transient Facility. We discuss the comprehensive data set in conjunction with a sample of previously reported, clearly double-peaked stripped-envelope supernovae from the ZTF archive, and for several of these, we also provide previously unpublished data. With data from one homogeneous survey, we can quantify some of the key properties of the double-peaked light curves, analyze correlations between these properties, and contextualize them with some of the common powering mechanisms that we review from the literature.

SN 2021lvy is a luminous and slowly evolving Type Ib supernova with both peaks reaching roughly the same brightness. Although it shows many similarities to SN 2019stc, with both having their first peaks fitting a combination of radioactive nickel power and magnetar central engine input, their second peaks diverge significantly in behavior.

SN 2021uvy shows a lack of color evolution during the second decline and a rise in photospheric temperature, which is a prediction in the case of variable thermal energy injection from magnetar spin-down (Moriya et al. 2022).

SN 2022hgk, on the other hand, is an average-luminosity Type Ib supernova with a much brighter second peak. Its light curve is very similar to the light curve of SN 2019cad, which is considered an analog of SN 2005bf (and also to PTF11mnb). The spectra of SN 2022hgk, however, show a significant similarity with those of SN 2005bf (strong helium absorption features) rather than with those of SN 2019cad. Overall, these four supernovae (SNe 2005bf, PTF11mnb, 2019cad, and 2022hgk) have similar light-curve parameters and form a tight group in the phase space of absolute peak magnitudes of the second peak versus that of the first peak and in the magnitude difference between the peaks versus the duration between the peaks. The double-nickel distribution powering mechanism might well fit this group of supernovae (see e.g., Orellana & Bersten 2022).

With a sample of double-peaked SESNe coming together (being $\sim 2.5\%$ of all Type Ibc SNe), it becomes clear that this is a phenomenon that requires a more holistic approach. There have been good arguments in the literature as to why some of these events should not be just random alignments of two distinct SNe, or even two separate stars exploding in a binary system, and with the expanding sample, such probability estimates gain more weight. At the same time, fine-tuned models to explain individual and very rare systems become less probable once it is realized that more of these systems exist. Upcoming facilities like the Rubin Observatory will increase the sample size of double-peaked and multi-peaked SESNe and also provide more light curve properties to help uncover their powering mechanisms with the depth of the Legacy Survey of Space and Time (LSST; Ivezić et al. 2019).

Acknowledgments

Based on observations obtained with the Samuel Oschin Telescope 48 inch and the 60 inch Telescope at the Palomar Observatory as part of the Zwicky Transient Facility project. ZTF is supported by the National Science Foundation under grant Nos. AST-1440341 and AST-2034437, and a collaboration including current partners Caltech, IPAC, the Oskar Klein Center at Stockholm University, the University of Maryland, University of California, Berkeley, the University of Wisconsin at Milwaukee, University of Warwick, Ruhr University Bochum, Cornell University, Northwestern University, and Drexel University. Operations are conducted by COO, IPAC, and UW. The ZTF forced-photometry service was funded under the Heising-Simons Foundation grant #12540303 (PI: Graham). SED Machine is based upon work supported by the

National Science Foundation under grant No. 1106171. This work was supported by the GROWTH project (Kasliwal et al. 2019) funded by the National Science Foundation under PIRE grant No. 1545949. The Gordon and Betty Moore Foundation, through both the Data-Driven Investigator Program and a dedicated grant, provided critical funding for SkyPortal. The Oskar Klein Centre was funded by the Swedish Research Council. Partially based on observations made with the Nordic Optical Telescope, operated by the Nordic Optical Telescope Scientific Association at the Observatorio del Roque de los Muchachos, La Palma, Spain, of the Instituto de Astrofísica de Canarias. Some of the data presented here were obtained with ALFOSC, which is provided by the Instituto de Astrofísica de Andalucía (IAA) under a joint agreement with the University of Copenhagen and NOT. Some of the data presented herein were obtained at the W. M. Keck Observatory, which is operated as a scientific partnership among the California Institute of Technology, the University of California, and NASA; the observatory was made possible by the generous financial support of the W. M. Keck Foundation. This work has made use of data from the Asteroid Terrestrial-impact Last Alert System (ATLAS) project. The Asteroid Terrestrial-impact Last Alert System (ATLAS) project is primarily funded to search for near earth asteroids through NASA grants NN12AR55G, 80NSSC18K0284, and 80NSSC18K1575; byproducts of the NEO search include images and catalogs from the survey area. The ATLAS science products have been made possible through the contributions of the University of Hawaii Institute for Astronomy, the Queen's University Belfast, the Space Telescope Science Institute, the South African Astronomical Observatory, and The Millennium Institute of Astrophysics (MAS), Chile. This research has made use of the NASA/IPAC Infrared Science Archive, which is funded by the National Aeronautics and Space Administration and operated by the California Institute of Technology. The Liverpool Telescope is operated on the island of La Palma by Liverpool John Moores University in the Spanish Observatorio del Roque de los Muchachos of the Instituto de Astrofísica de Canarias with financial support from the UK Science and Technology Facilities Council.

Y.S. thanks the LSSTC Data Science Fellowship Program, which is funded by LSSTC, NSF Cybertraining grant #1829740, the Brinson Foundation, and the Moore Foundation; her participation in the program has benefited this work.

M.W.C. acknowledges support from the National Science Foundation with grant Nos. PHY-2308862 and PHY-2117997.

Fritz (van der Walt et al. 2019; Coughlin et al. 2023) and GROWTH marshal (Kasliwal et al. 2019) (dynamic collaborative platforms for time-domain astronomy) were used in this work.

Appendix A

Photometry Data

Photometric observations of SNe 2021uvy and 2022hgk presented in this paper are provided in Table 4 (optical) and Table 5 (UV).

Table 4

Log of Optical Photometry of SN 2021uvy and SN 2022hgk of $>5\sigma$ Significance and Corrected for MW Extinction (Full Table Available online, DOI:[10.5281/zenodo.15786071](https://doi.org/10.5281/zenodo.15786071))

IAU Name	MJD	Filter	Telescope	Brightness (mag)
SN 2021uvy	59401.44	<i>r</i>	P48:ZTF	20.85 ± 0.24
...
SN 2022hgk	59672.32	<i>g</i>	P48:ZTF	21.56 ± 0.22
...

Table 5

Log of UVOT Observations of SN 2022hgk of $>3\sigma$ Significance and Corrected for MW Extinction (Full Table Available online, DOI:[10.5281/zenodo.15786071](https://doi.org/10.5281/zenodo.15786071))

MJD	Filter	Brightness (mag)
59720.72	uvw2	19.625 ± 0.075
...

Appendix B Spectroscopy Data



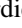
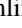




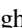




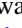





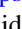




Optical spectroscopic observations of SNe 2020acct, 2021pkd, 2021uvy, 2022hgk, and 2023plg presented in this paper are summarized in Table 6.

Table 6
Summary of Optical Spectra of SNe 2020acct, 2021pkd, 2021uvy, 2022hgk, and 2023plg

IAU Name	MJD	Phase (day)	Telescope/Instrument	Exposure (s)	IAU Name	MJD	Phase (day)	Telescope/Instrument	Exposure (s)
SN 2020acct	59195	−1 (1)	P60/SEDm	2700	SN 2022hgk	59708	17 (33)	LT/SPRAT	600
	59253	55 (58)	P200/DBSP	450		59709	18 (34)	P60/SEDm	2700
	59254	56 (59)	P60/SEDm	2700		59710	19 (35)	NOT/ALFOSC	3600
	59255	57 (60)	NOT/ALFOSC	1350		59713	22 (38)	P60/SEDm	2700
	59256	58 (61)	P60/SEDm	2700		59718	27 (43)	P60/SEDm	2700
	59260	62 (65)	NOT/ALFOSC	900		59719	28 (44)	P60/SEDm	2700
	59260	62 (65)	P60/SEDm	2700		59721	30 (46)	NOT/ALFOSC	1800
	59263	64 (67)	Keck1/LRIS	1275		59722	31 (47)	P200/DBSP	1200
	59277	78 (81)	NOT/ALFOSC	1800		59730	39 (55)	P60/SEDm	2700
	59311	112 (114)	Keck1/LRIS	2312		59732	40 (56)	NOT/ALFOSC	2400
SN 2021pkd	59350	149 (152)	Keck1/LRIS	2705		59734	43 (59)	P60/SEDm	2700
						59738	46 (62)	P200/DBSP	1500
	59386	−7 (12)	P60/SEDm	2700		59739	47 (63)	P200/DBSP	900
	59389	−4 (15)	P60/SEDm	2700		59788	95 (111)	Keck1/LRIS	900
	59391	−3 (17)	P60/SEDm	2700	SN 2023plg	60242	70 (70)	P60/SEDm	2700
SN 2021uvy	59401	7 (26)	Keck1/LRIS	300		60246	74 (74)	LT/SPRAT	750
						60246	74 (74)	P60/SEDm	2160
	59439	−15 (38)	NTT/EFOSC2	900		60249	77 (77)	P60/SEDm	2160
	59442	−12 (40)	P60/SEDm	2700		60254	82 (82)	P60/SEDm	2160
	59454	−1 (51)	P60/SEDm	2700		60256	84 (84)	Keck1/LRIS	300
	59455	0 (52)	LT/SPRAT	750		60259	87 (87)	P60/SEDm	2160
	59458	2 (55)	P200/DBSP	600		60269	97 (97)	P60/SEDm	2700
	59467	10 (62)	Keck1/LRIS	600		60274	102 (102)	P60/SEDm	2700
	59467	11 (63)	P60/SEDm	2700		60275	102 (102)	NOT/ALFOSC	2400
	59470	13 (66)	P200/DBSP	900		60280	107 (107)	P60/SEDm	2760
	59491	33 (85)	Keck1/LRIS	600		60281	108 (108)	P60/SEDm	2760
	59498	39 (91)	P60/SEDm	2700		60281	108 (108)	P200/DBSP	1200
	59502	43 (95)	P60/SEDm	2700		60282	109 (109)	P60/SEDm	3624
	59509	49 (101)	P60/SEDm	2700		60283	110 (110)	P60/SEDm	396
	59517	57 (109)	P60/SEDm	2700		60285	112 (112)	P60/SEDm	2700
	59524	63 (115)	P200/DBSP	900		60285	112 (112)	P60/SEDm	3840
	59536	74 (126)	P60/SEDm	2700		60286	113 (113)	NOT/ALFOSC	2400
	59547	84 (136)	P60/SEDm	2700		60288	115 (115)	P60/SEDm	2700
	59561	97 (149)	P60/SEDm	2700		60296	123 (123)	P60/SEDm	2700
	59585	118 (171)	P60/SEDm	2700		60299	126 (126)	NOT/ALFOSC	1200
	59587	120 (172)	NOT/ALFOSC	2700		60321	147 (147)	NOT/ALFOSC	2400
	59600	132 (185)	P60/SEDm	2700					
	59615	146 (198)	Keck1/LRIS	300					
	59815	328 (380)	Keck1/LRIS	1800					
	59875	384 (436)	Keck1/LRIS	2700					

Note. We report phases (in rest-frame days) calculated with respect to both the first peak of the light curve and the estimated explosion epoch (inside parentheses).

ORCID iDs

Yashvi Sharma  <https://orcid.org/0000-0003-4531-1745>
 Jesper Sollerman  <https://orcid.org/0000-0003-1546-6615>
 William Meynardie  <https://orcid.org/0009-0001-6903-0131>
 Christoffer Fremling  <https://orcid.org/0000-0002-4223-103X>
 Kaustav K. Das  <https://orcid.org/0000-0001-8372-997X>
 Gene Yun  <https://orcid.org/0009-0001-3390-5151>
 S. R. Kulkarni  <https://orcid.org/0000-0001-5390-8563>
 Steve Schulze  <https://orcid.org/0000-0001-6797-1889>
 Jacob Wise  <https://orcid.org/0000-0003-0733-2916>
 Seán J. Brennan  <https://orcid.org/0000-0003-1325-6235>
 Thomas G. Brink  <https://orcid.org/0000-0001-5955-2502>
 Michael W. Coughlin  <https://orcid.org/0000-0002-8262-2924>
 Richard Dekany  <https://orcid.org/0000-0002-5884-7867>
 Matthew J. Graham  <https://orcid.org/0000-0002-3168-0139>
 K. R. Hinds  <https://orcid.org/0000-0002-0129-806X>
 Viraj Karambelkar  <https://orcid.org/0000-0003-2758-159X>
 Mansi M. Kasliwal  <https://orcid.org/0000-0002-5619-4938>
 Maggie L. Li  <https://orcid.org/0009-0001-6911-9144>
 Kira Nolan  <https://orcid.org/0009-0002-4724-7118>
 Daniel A. Perley  <https://orcid.org/0000-0001-8472-1996>
 Josiah N. Purdum  <https://orcid.org/0000-0003-1227-3738>
 Sam Rose  <https://orcid.org/0000-0003-4725-4481>
 Ben Rusholme  <https://orcid.org/0000-0001-7648-4142>
 Tawny Sit  <https://orcid.org/0000-0001-8208-9755>
 Anastasios Tzanidakis  <https://orcid.org/0000-0003-0484-3331>
 Avery Wold  <https://orcid.org/0000-0002-9998-6732>
 Lin Yan  <https://orcid.org/0000-0003-1710-9339>
 Yuhao Yao  <https://orcid.org/0000-0001-6747-8509>

References

- Angus, C. R., Woosley, S. E., Foley, R. J., et al. 2024, *ApJL*, **977**, L41
 Anupama, G. C., Sahu, D. K., Deng, J., et al. 2005, *ApJL*, **631**, L125
 Arnett, W. D. 1982, *ApJ*, **253**, 785
 Astropy Collaboration, Price-Whelan, A. M., Lim, P. L., et al. 2022, *ApJ*, **935**, 167
 Barbary, K. 2016, extinction v0.3.0, Zenodo, doi:10.5281/zenodo.804967
 Barkat, Z., Rakavy, G., & Sack, N. 1967, *PhRvL*, **18**, 379
 Barmantloo, S., Jerkstrand, A., Iwamoto, K., et al. 2024, *MNRAS*, **533**, 1251
 Becker, A., 2015 HOTPANTS: High Order Transform of PSF ANd Template Subtraction, Astrophysics Source Code Library, ascl:1504.004
 Bellm, E. C., Kulkarni, S. R., Barlow, T., et al. 2019, *PASP*, **131**, 068003
 Ben-Ami, S., Konidaris, N., Quimby, R., et al. 2012, *Proc. SPIE*, **8446**, 844686
 Bersten, M. C., Tanaka, M., Tominaga, N., Benvenuto, O. G., & Nomoto, K. 2013, *ApJ*, **767**, 143
 Blagorodnova, N., Neill, J. D., Walters, R., et al. 2018, *PASP*, **130**, 035003
 Blondin, S., & Tonry, J. L. 2007, *ApJ*, **666**, 1024
 Breeveld, A. A., Landsman, W., Holland, S. T., et al. 2011, in AIP Conf. Ser. 1358, ed. J. E. McEnery, J. L. Racusin, & N. Gehrels (Melville, NY: AIP), 373
 Buzzoni, B., Delabre, B., Dekker, H., et al. 1984, *Mnrg*, **38**, 9
 Cartier, R., Contreras, C., Stritzinger, M., et al. 2024, arXiv:2410.21381
 Cenko, S. B., Fox, D. B., Moon, D.-S., et al. 2006, *PASP*, **118**, 1396
 Chen, P., Gal-Yam, A., Sollerman, J., et al. 2024, *Natur*, **625**, 253
 Chen, T.-W. 2019, The Extragalactic Explosive Universe: the New Era of Transient Surveys and Data-Driven Discovery, **15**, Version v1
 Chen, Z. H., Yan, L., Kangas, T., et al. 2023a, *ApJ*, **943**, 41
 Chen, Z. H., Yan, L., Kangas, T., et al. 2023b, *ApJ*, **943**, 42
 Chiba, R., & Moriya, T. J. 2024, *ApJ*, **973**, 14
 Chu, M., Dahiwal, A., & Fremling, C. 2021, *TNSCR*, **2021**, 1
 Chugai, N. N., & Utrobin, V. P. 2022, *MNRAS*, **512**, L71
 Coughlin, M. W., Bloom, J. S., Nir, G., et al. 2023, *ApJS*, **267**, 31
 Crawford, A., Pritchard, T. A., Modjaz, M., et al. 2025, *ApJ*, **989**, 192
 Das, K. K., Kasliwal, M. M., Sollerman, J., et al. 2024, *ApJ*, **972**, 91
 Dekany, R., Smith, R. M., Riddle, R., et al. 2020, *PASP*, **132**, 038001
 Dey, A., Schlegel, D. J., Lang, D., et al. 2019, *AJ*, **157**, 168
 Dong, X.-F., Liu, L.-D., Gao, H., & Yang, S. 2023, *ApJ*, **951**, 61
 Fang, Q., Maeda, K., Kuncarayakti, H., Sun, F., & Gal-Yam, A. 2019, *NatAs*, **3**, 434
 Fitzpatrick, E. L. 1999, *PASP*, **111**, 63
 Folatelli, G., Contreras, C., Phillips, M. M., et al. 2006, *ApJ*, **641**, 1039
 Fremling, C. 2021, *TNSR*, **2021**, 1
 Fremling, C. 2022, *TNSR*, **2022**, 1
 Fremling, C., Miller, A. A., Sharma, Y., et al. 2020, *ApJ*, **895**, 32
 Fremling, C., Sollerman, J., Taddia, F., et al. 2016, *A&A*, **593**, A68
 Galama, T. J., Vreeswijk, P. M., van Paradijs, J., et al. 1998, *Natur*, **395**, 670
 Gehrels, N., Chincarini, G., Giommi, P., et al. 2004, *ApJ*, **611**, 1005
 Gomez, S., Berger, E., Hosseinzadeh, G., et al. 2021, *ApJ*, **913**, 143
 Gomez, S., Berger, E., Nicholl, M., Blanchard, P. K., & Hosseinzadeh, G. 2022, *ApJ*, **941**, 107
 Graham, M. J., Kulkarni, S. R., Bellm, E. C., et al. 2019, *PASP*, **131**, 078001
 Gutiérrez, C. P., Bersten, M. C., Orellana, M., et al. 2021, *MNRAS*, **504**, 4907
 Hunter, J. D. 2007, *CSE*, **9**, 90
 Ivezić, Ž., Kahn, S. M., Tyson, J. A., et al. 2019, *ApJ*, **873**, 111
 Jin, H., Yoon, S.-C., & Blinnikov, S. 2021, *ApJ*, **910**, 68
 Kangas, T., Kuncarayakti, H., Nagao, T., et al. 2024, *A&A*, **689**, A182
 Karamehmetoglu, E., Sollerman, J., Taddia, F., et al. 2023, *A&A*, **678**, A87
 Kasliwal, M. M., Cannella, C., Bagdasaryan, A., et al. 2019, *PASP*, **131**, 038003
 Khatami, D. K., & Kasen, D. N. 2019, *ApJ*, **878**, 56
 Khatami, D. K., & Kasen, D. N. 2024, *ApJ*, **972**, 140
 Kim, Y. L., Rigault, M., Neill, J. D., et al. 2022, *PASP*, **134**, 024505
 Kuncarayakti, H., Maeda, K., Bersten, M. C., et al. 2015, *A&A*, **579**, A95
 Kuncarayakti, H., Sollerman, J., Izzo, L., et al. 2023, *A&A*, **678**, A209
 Leung, S.-C., Nomoto, K., & Blinnikov, S. 2019, *ApJ*, **887**, 72
 Lunnan, R., Chornock, R., Berger, E., et al. 2016, *ApJ*, **831**, 144
 Lunnan, R., Yan, L., Perley, D. A., et al. 2021, *TNSAN*, **218**, 1
 Maeda, K., Tanaka, M., Nomoto, K., et al. 2007, *ApJ*, **666**, 1069
 Masci, F. J., Laher, R. R., Rusholme, B., et al. 2019, *PASP*, **131**, 018003
 Masci, F. J., Laher, R. R., Rusholme, B., et al. 2023, arXiv:2305.16279
 Milisavljevic, D., Fesen, R. A., Gerardy, C. L., Kirshner, R. P., & Challis, P. 2010, *ApJ*, **709**, 1343
 Moore, T., Smartt, S. J., Nicholl, M., et al. 2023, *ApJL*, **956**, L31
 Morales-Garoffolo, A., Elias-Rosa, N., Bersten, M., et al. 2015, *MNRAS*, **454**, 95
 Moriya, T. J., Murase, K., Kashiyama, K., & Blinnikov, S. I. 2022, *MNRAS*, **513**, 6210
 Nakar, E., & Piro, A. L. 2014, *ApJ*, **788**, 193
 Nicholl, M. 2018, *RNAAS*, **2**, 230
 Oke, J. B., Cohen, J. G., Carr, M., et al. 1995, *PASP*, **107**, 375
 Oke, J. B., & Gunn, J. E. 1982, *PASP*, **94**, 586
 Orellana, M., & Bersten, M. C. 2022, *A&A*, **667**, A92
 Patat, F., Cappellaro, E., Danziger, J., et al. 2001, *ApJ*, **555**, 900
 Pellegrino, C., Hiramatsu, D., Arcavi, I., et al. 2023, *ApJ*, **954**, 35
 Perley, D., Chu, M., Dahiwal, A., & Fremling, C. 2022, *TNSCR*, **2022**, 1
 Perley, D. A. 2019, *PASP*, **131**, 084503
 Perley, D. A., Fremling, C., Sollerman, J., et al. 2020, *ApJ*, **904**, 35
 Piascik, A. S., Steele, I. A., Bates, S. D., et al. 2014, *Proc. SPIE*, **9147**, 91478H
 Piro, A. L. 2015, *ApJL*, **808**, L51
 Piro, A. L., Haynie, A., & Yao, Y. 2021, *ApJ*, **909**, 209
 Planck Collaboration, Aghanim, N., Akrami, Y., et al. 2020, *A&A*, **641**, A6
 Poidevin, F., Perez-Fournon, I., Angel, C. J., et al. 2021, *TNSCR*, **2021**, 1
 Prentice, S. J., Ashall, C., James, P. A., et al. 2019, *MNRAS*, **485**, 1559

- Prentice, S. J., Maguire, K., Siebenaler, L., & Jerkstrand, A. 2022, *MNRAS*, **514**, 5686
- Prochaska, J. X., Hennawi, J. F., Westfall, K. B., et al. 2020, *JOSS*, **5**, 2308
- Rakavy, G., Shaviv, G., & Zinamon, Z. 1967, *ApJ*, **150**, 131
- Rehmtulla, N., Miller, A. A., Jegou Du Laz, T., et al. 2024, *ApJ*, **972**, 7
- Ridley, E., Gompertz, B., Nicholl, M., Galbany, L., & Yaron, O. 2021, *TNSCR*, **1**, 2021
- Rigault, M., Neill, J. D., Blagorodnova, N., et al. 2019, *A&A*, **627**, A115
- Roberson, M., Fremling, C., & Kasliwal, M. 2022, *JOSS*, **7**, 3612
- Rodríguez, Ó., Maoz, D., & Nakar, E. 2023, *ApJ*, **955**, 71
- Rodríguez, Ó., Nakar, E., & Maoz, D. 2024, *Natur*, **628**, 733
- Roming, P. W. A., Kennedy, T. E., Mason, K. O., et al. 2005, *SSRv*, **120**, 95
- Schlafly, E. F., & Finkbeiner, D. P. 2011, *ApJ*, **737**, 103
- Schulze, S., Fransson, C., Kozyreva, A., et al. 2024, *A&A*, **683**, A223
- Sharma, Y., Sollerman, J., Kulkarni, S. R., et al. 2024, *ApJ*, **966**, 199
- Shivvers, I., Filippenko, A. V., Silverman, J. M., et al. 2019, *MNRAS*, **482**, 1545
- Smartt, S. J., Valenti, S., Fraser, M., et al. 2015, *A&A*, **579**, A40
- Smith, K. W., Smartt, S. J., Young, D. R., et al. 2020, *PASP*, **132**, 085002
- Sollerman, J., Fransson, C., Barbarino, C., et al. 2020, *A&A*, **643**, A79
- Sollerman, J., Holland, S. T., Challis, P., et al. 2002, *A&A*, **386**, 944
- Sollerman, J., Yang, S., Perley, D., et al. 2022, *A&A*, **657**, A64
- Soraisam, M., Matheson, T., Lee, C.-H., et al. 2022, *ApJL*, **926**, L11
- Steele, I. A., Smith, R. J., Rees, P. C., et al. 2004, *Proc. SPIE*, **5489**, 679
- Taddia, F., Fremling, C., Sollerman, J., et al. 2016, *A&A*, **592**, A89
- Taddia, F., Sollerman, J., Fremling, C., et al. 2018, *A&A*, **609**, A106
- Taddia, F., Sollerman, J., Leloudas, G., et al. 2015, *A&A*, **574**, A60
- Takei, Y., & Tsuna, D. 2024, *OJAp*, **7**, 119
- Tartaglia, L., Sollerman, J., Barbarino, C., et al. 2021, *A&A*, **650**, A174
- Taubenberger, S., Valenti, S., Benetti, S., et al. 2009, *MNRAS*, **397**, 677
- Tonry, J. L., Denneau, L., Heinze, A. N., et al. 2018, *PASP*, **130**, 064505
- van der Walt, S., Colbert, S. C., & Varoquaux, G. 2011, *CSE*, **13**, 22
- van der Walt, S. J., Crellin-Quick, A., & Bloom, J. S. 2019, *JOSS*, **4**, 1247
- Virtanen, P., Gommers, R., Oliphant, T. E., et al. 2020, *NatMe*, **17**, 261
- Woosley, S. E. 2017, *ApJ*, **836**, 244
- Woosley, S. E., Sukhbold, T., & Kasen, D. N. 2021, *ApJ*, **913**, 145
- Yang, S., & Sollerman, J. 2023, *ApJS*, **269**, 40
- Yaron, O., & Gal-Yam, A. 2012, *PASP*, **124**, 668
- Zhu, J.-P., Liu, L.-D., Yu, Y.-W., et al. 2024, *ApJL*, **970**, L42